AFRL-IF-RS-TR-2003-53
Final Technical Report
March 2003

THROUGH THE WALL IMAGING RADAR

AKELA, Incorporated

APPROVED FOR PUBLIC RELEASE; DISTRIBUTION UNLIMITED.

AIR FORCE RESEARCH LABORATORY
INFORMATION DIRECTORATE
ROME RESEARCH SITE
ROME, NEW YORK

This report has been reviewed by the Air Force Research Laboratory, Information Directorate, Public Affairs Office (IFOIPA) and is releasable to the National Technical Information Service (NTIS). At NTIS it will be releasable to the general public, including foreign nations.

AFRL-IF-RS-TR-2003-53 has been reviewed and is approved for publication.

APPROVED: 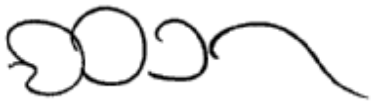

DAVID D. FERRIS
Project Engineer

FOR THE DIRECTOR: 

JOSEPH CAMERA, Chief
Information & Intelligence Exploitation Division
Information Directorate

REPORT DOCUMENTATION PAGE

Form Approved
OMB No. 074-0188

1. AGENCY USE ONLY (Leave blank)	2. REPORT DATE	3. REPORT TYPE AND DATES COVERED
	MARCH 2003	Final Aug 00 – Aug 02

4. TITLE AND SUBTITLE
THROUGH THE WALL IMAGING RADAR

5. FUNDING NUMBERS
C - F30602-00-C-0205
PE - N/A
PR - CWDP
TA - 00
WU - 02

6. AUTHOR(S)
Allan Hunt

7. PERFORMING ORGANIZATION NAME(S) AND ADDRESS(ES)
AKELA, Incorporated
5276 Hollister Avenue
Suite 263
Santa Barbara California 93111

8. PERFORMING ORGANIZATION REPORT NUMBER

9. SPONSORING / MONITORING AGENCY NAME(S) AND ADDRESS(ES)
Air Force Research Laboratory/IFEA
32 Brooks Road
Rome New York 13441-4114

10. SPONSORING / MONITORING AGENCY REPORT NUMBER
AFRL-IF-RS-TR-2003-53

11. SUPPLEMENTARY NOTES

AFRL Project Engineer: David D. Ferris/IFEA/(315) 330-4408/ David.Ferris@rl.af.mil

12a. DISTRIBUTION / AVAILABILITY STATEMENT
APPROVED FOR PUBLIC RELEASE; DISTRIBUTION UNLIMITED.

12b. DISTRIBUTION CODE

13. ABSTRACT ***(Maximum 200 Words)***

This effort was established to develop a dual mode stepped frequency radar and advanced image recognition processing. The first mode would be used to image walls within a building. This imagery would allow a building to be remotely mapped. The second mode would be used to detect the presence of living people within the building. The task would then continue by working to integrate the imagery of the living people with the imagery of the building.

A brassboard antenna array and radar electronics were integrated into a collapsing structure that weighs less than 20 pounds and is small enough to be carried by a single individual. The radar is capable of seeing through walls and forming images of the structure as well as detecting individuals at a range of 40 feet. The brassboard can be used to detect the motion of individuals through multiple interior walls using coherent scene subtraction. The images formed by the radar will improve tactical awareness in operational environments.

14. SUBJECT TERMS	15. NUMBER OF PAGES
Stepped Frequency Radar, Imaging Radar	65
	16. PRICE CODE

17. SECURITY CLASSIFICATION OF REPORT	18. SECURITY CLASSIFICATION OF THIS PAGE	19. SECURITY CLASSIFICATION OF ABSTRACT	20. LIMITATION OF ABSTRACT
UNCLASSIFIED	UNCLASSIFIED	UNCLASSIFIED	UL

Table of Contents

List of Figures

There is no Figure 47.

Introduction

There are many situations in both peace keeping and law enforcement operations where there is a need to not only determine if there is someone inside a building structure but also to know where they are. These situations arise during searches for suspects, hostage and barricade incidents, and tactical surveillance. While in many cases the objective is to make contact with a suspect to defuse a potentially violent situation, not all suspects are cooperative. This often leads to the necessity of entering a building in order to take a suspect into custody. Unfortunately, most operations conclude with a physical search with personnel under a great deal of stress and subject to a high possibility of physical harm.

The technology available to peace keeping and law enforcement personnel to assist them in apprehending a suspect is rapidly changing. A new generation of techniques is being developed that will enhance the capability to look into buildings at standoff distances and build a picture of the tactical situation. Knowing that there is someone inside a building, where they are inside, and what the internal layout of the building is, will change the operational tactics used and increase the probability that an operation will successfully conclude without casualties.

The activities performed by AKELA under contract F30602-00-C-0205 have been designed to meet this operational need for better tactical surveillance information. We have demonstrated the capability of a portable, compact radar to reconstruct an image of the interior structure of a building, and to detect the motion of individuals both through multiple internal walls and reinforced concrete exterior walls. Our radar uses a stationary, multiple antenna array and microwave tomographic image reconstruction algorithms to produce a two dimensional picture of the structure and to show motion within. Figure 1 is a picture of the brassboard radar system that was developed for this program.

As shown in Figure 1, the imaging radar sensor array is 2.2 m wide when fully extended and collapses to a size approximately 16” wide, 25” long, and 14” tall. It weighs less than 20 pounds and operates on battery power for up to about 8 hours. The radar control and display functions are performed by an off the shelf desktop or laptop computer. This system is easily portable and quickly put in place - both features that are operationally significant.

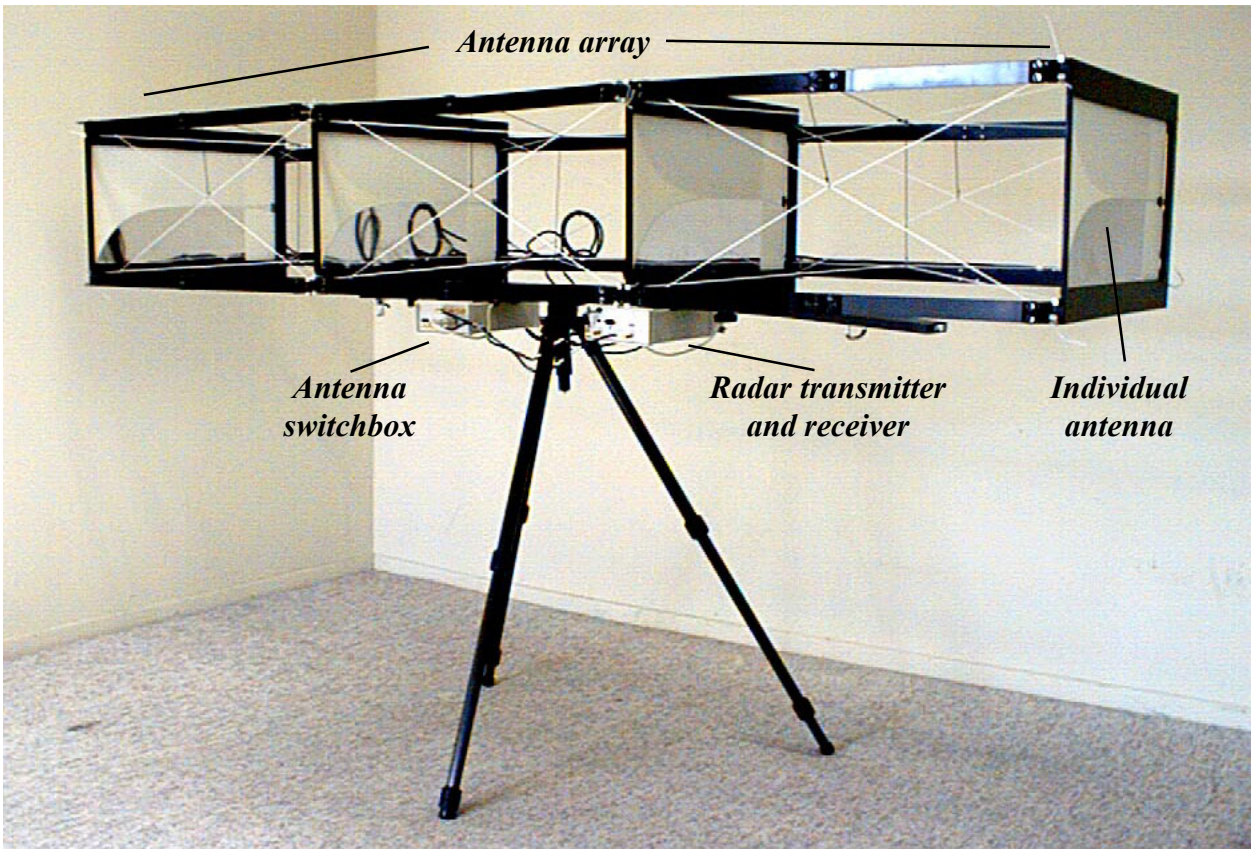

Figure 1 - Through the wall imaging radar system brassboard.

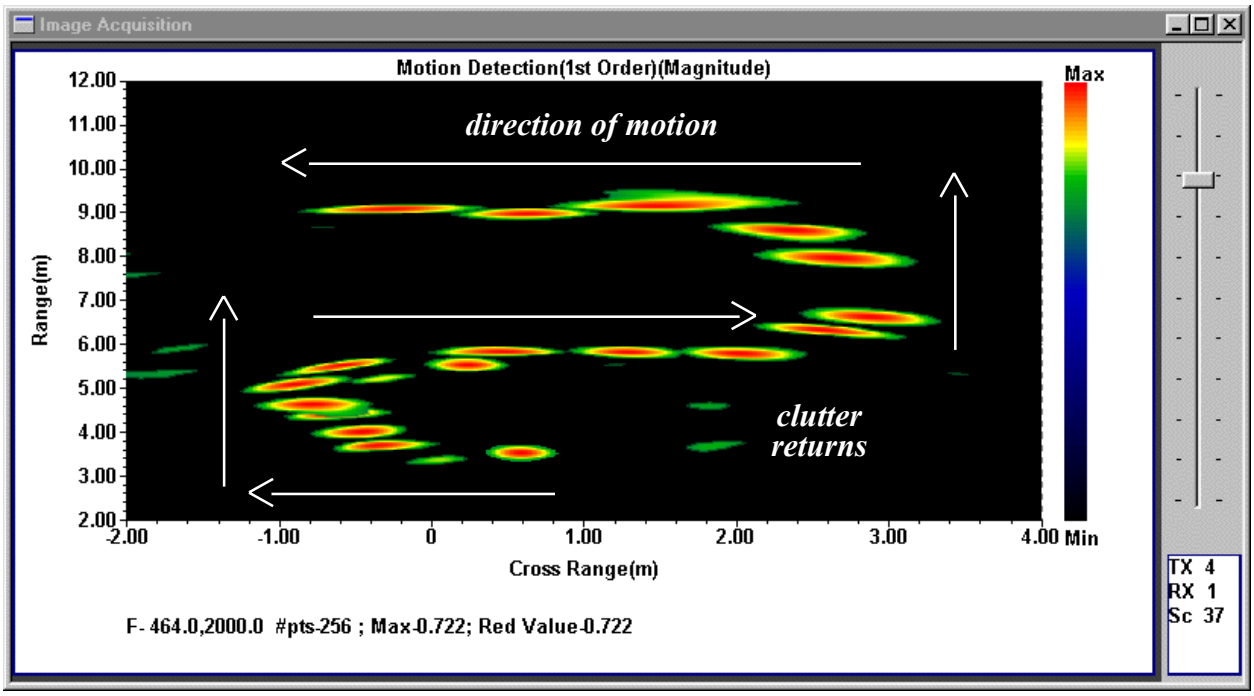

Figure 2 - Composite image of motion of a person walking behind interior walls.

The brassboard has been used in the field to collect data on its motion detection and imaging capabilities. Figure 2 shows a composite image from a motion detection experiment. In the experiment, there are two parallel, 2.4 m x 2.4 m (8 ft x 8 ft) stud walls faced with drywall, positioned horizontally 4.6 m and 7.2 m in front of the brassboard, with their left edges at 0 m. An individual started out walking to the left in the image in front of the closest wall, proceeded to walk around the left edge of the wall and then to the right behind it and in front of the second wall. Upon reaching the right edge of the parallel walls, the individual then turned to the left and walked back in the opposite direction behind both walls. The walls do not show up in the composite image because motion is detected by using coherent scene subtraction. Since the walls do not move, they become part of the background that gets removed when subsequent image frames are subtracted.

Figure 3 shows an image from a series of tests designed to investigate the resolution enhancement that can be obtained by using a longer array with more antennas. While this experiment used a single array with 8 antennas, using two shorter arrays and combining their output would yield similar results. In this experiment, there were two horizontal walls parallel to the imaging radar, connected at one end by another wall perpendicular to the other two walls, thus forming an

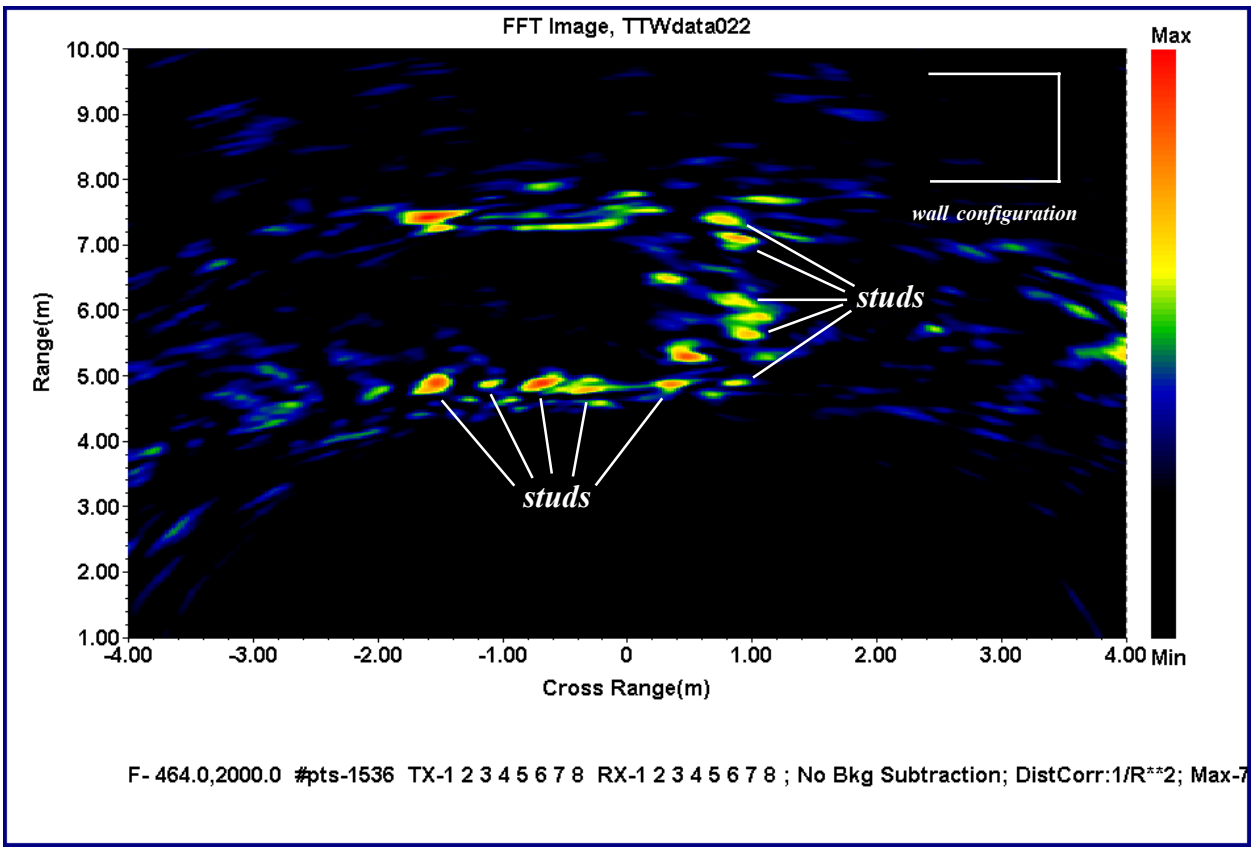

Figure 3 - High resolution image formation.

open ended room. The image shows individual studs in the walls and the overall shape of the open ended room is clearly evident.

During the same set of tests, the walls were reconfigured so that they were parallel to one another and the imaging radar. Figure 4 shows an image of a person standing at a distance of 12 meters behind all three walls. In this case there is also a calibration sphere that was positioned between the first and second wall with the "shadow" of the sphere showing up on the surface of the second wall.

While a set of experiments aimed at determining the maximum detection range of the brassboard sensor through walls was never performed, a set of experiments performed cooperatively with another AFRL effort shows that the sensor has sufficient sensitivity to detect people at the maximum range limit of 30 meters (100 feet) specified by the contract. This set of experiments was designed to determine the capability of the imaging radar to detect individuals through

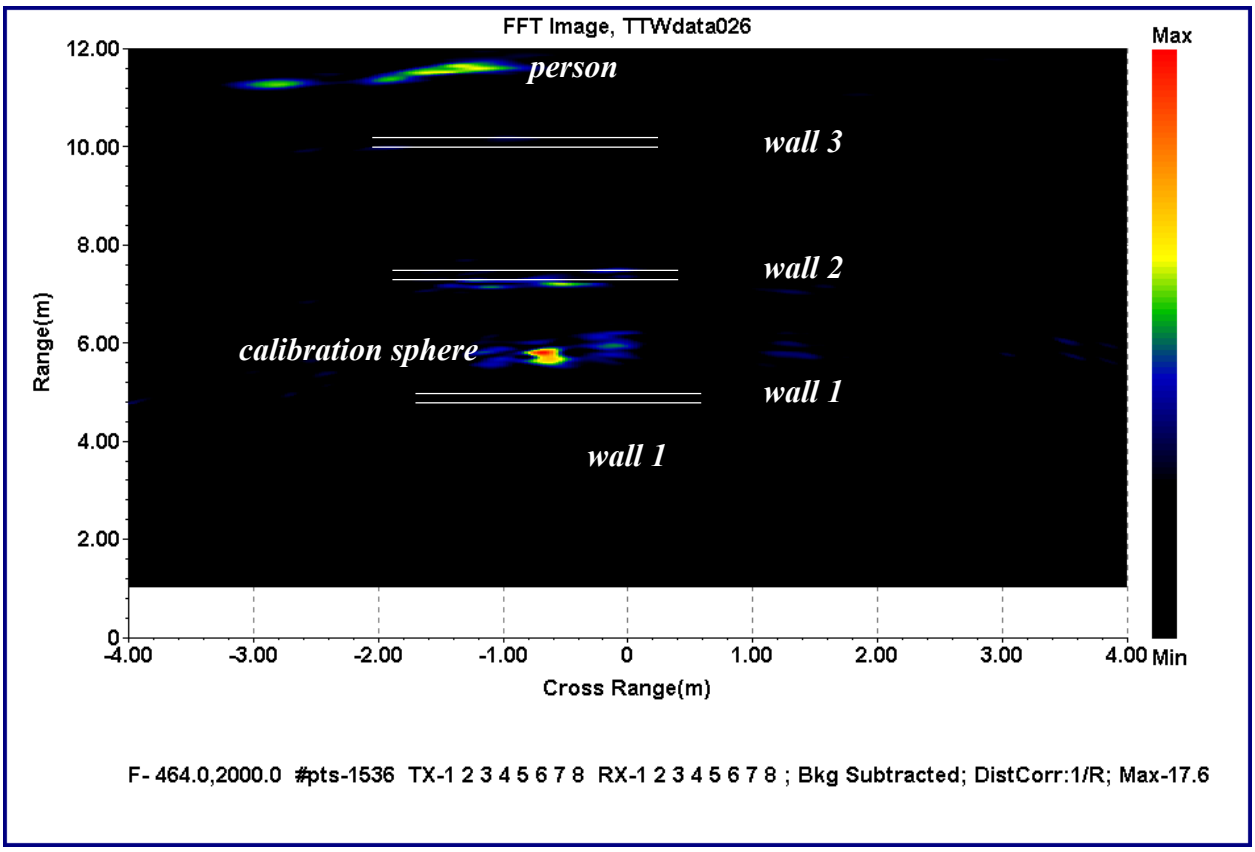

Figure 4 - Person imaged through three walls.

foliage. Figure 5 is an image of a person at a slant range of 40 meters from the radar. The person was imaged through 25 meters of moderately spaced, dense, woody brush. As seen in the figure, the person shows up quite readily.

Finally, experiments were performed to determine the capability of the brassboard radar to image and detect motion through exterior walls made of steel reinforced concrete. While it appears that the brassboard will detect motion through this type of wall, the images that were obtained were poor.

The objectives of our program have been met. We have developed a brassboard system that is field portable. It will produce images of the interior of a building structure. It can detect the motion of individuals through multiple walls. And it is sensitive enough to work at ranges up to 100 feet. The images and motion that we show with our system appear to be acceptable operationally. However, they can not be produced in an operationally relevant time scale.

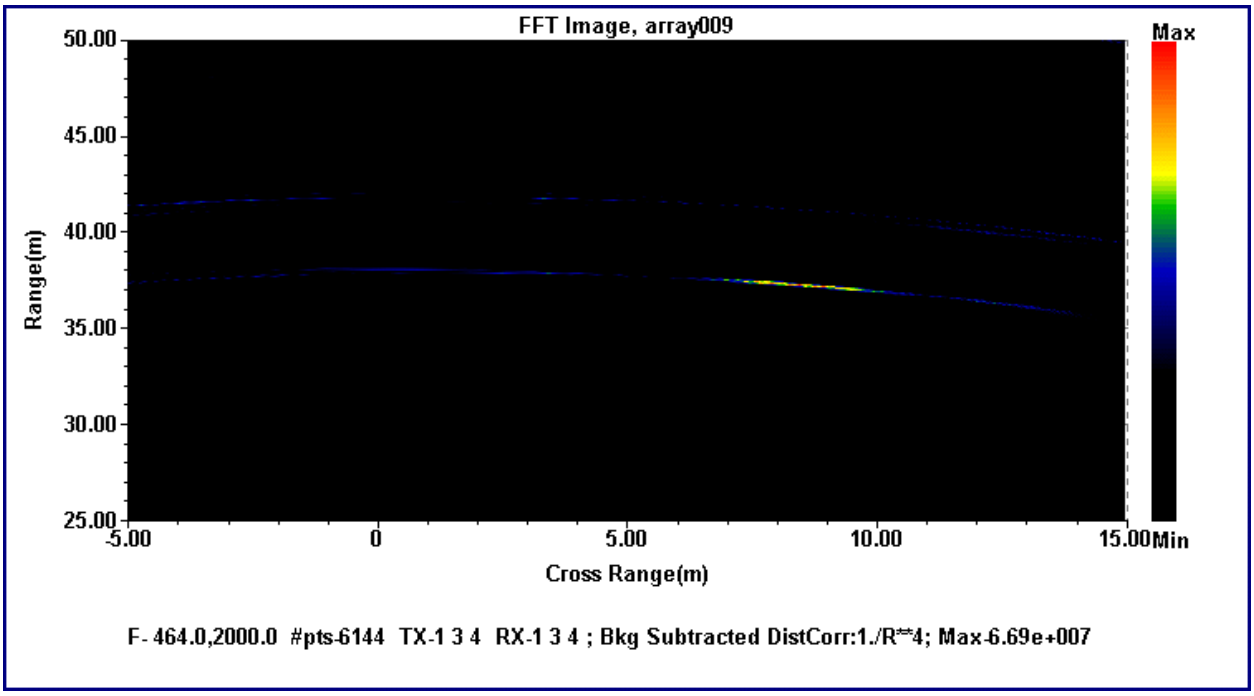

Figure 5 - Person imaged at 40 meters through dense brush.

This operational limitation is imposed primarily by the radar that was used to develop the brass-board. Since the radar was originally designed for the purpose of detecting concealed weapons, its operating parameters are not optimized for through-the-wall imaging applications. The current state of electronics technology is adequate to support the development of an imaging radar that would meet operational requirements.

Background/Theory of Operation

In order to create an image of the interior of an object, the illuminating radiation must be able to pass through the object with little attenuation. For through the wall surveillance systems the material properties of the wall determine the degree to which the system will be successful. The major considerations are the absorption and refraction losses for the penetrating radiation. Data taken by Frazier[1] show that most building materials are relatively transparent below 4 GHz. A graph that summarizes the one way attenuation loss through different types of materials is shown in Figure 6. For the case of reinforced concrete walls, Frazier made measurements at frequencies between 100 MHz and 2.5 GHz, finding that attenuation was moderate up to 2 GHz before

1. L. Frazier, "MDR for Law Enforcement", IEEE Potentials, Vol. 16, No. 5, pp. 23 - 26, 1998

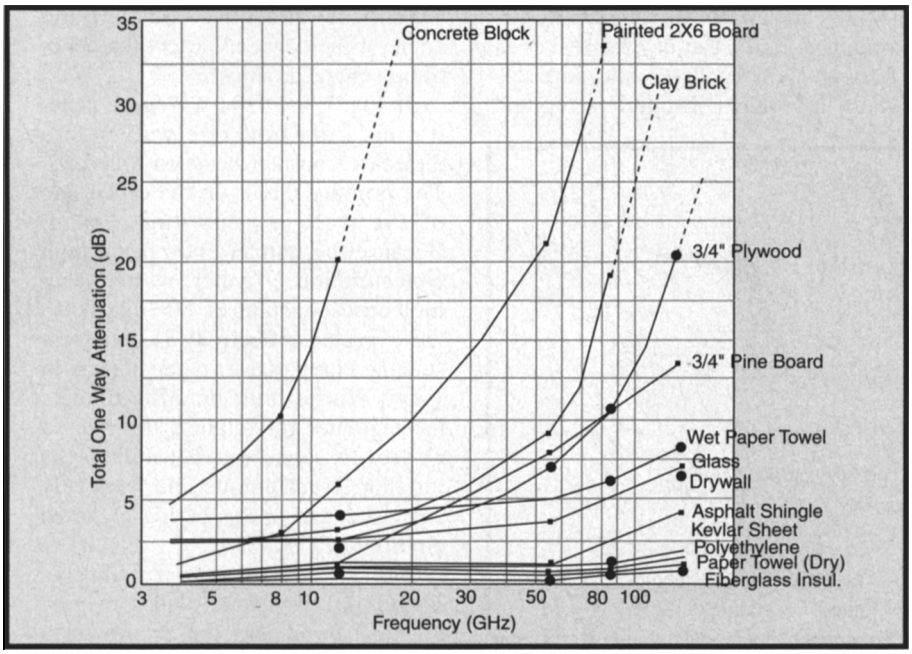

Figure 6 - Attenuation of common building materials. [1]

beginning to increase rapidly. A through the wall surveillance system that uses frequencies below 2 GHz appears to have the best chance of meeting the requirements for peacekeeping and law enforcement operations.

Tomographic image reconstruction is the method that is most often used to create images of the interior of an object. It is most widely known for its use in the field of medicine. While the type of energy used to probe the object varies, the basic method of reconstructing an image of the inside of the object consists of collecting data over a range of orientations and using backward propagation algorithms to remove ambiguities in the location of objects that scatter the probing radiation. In this way, a picture of the inside of the object showing the relative location of scattering objects is formed.

To achieve two dimensional image reconstruction requires being able to resolve scattering objects in both the range and cross range directions. The methods used vary, depending on the method of illumination and the nature of the radiation. For a stepped frequency waveform, range resolution is determined by the bandwidth of the waveform and follows the relation $\Delta R = c/2n\Delta f$, where c is the speed of light, n the number of frequency steps in the waveform, and Δf is the frequency step size. As with pulsed radar waveforms, there is range ambiguity associated with a

stepped frequency waveform. The unambiguous range limit $R_u = c/2\Delta f$. Fourier transforming the collected spectral information produces a range profile. Unfortunately, scatterers at ranges greater than the range limit will fold over and appear in the range profile.

For the radar system used on this program, the total bandwidth is 1.5 GHz, making the size of a resolvable range cell 0.1 meters (3.9 inches). The unambiguous range limit for a waveform of 1024 points is 102.4 meters. Reducing the number of points over the same bandwidth decreases the range limit. Reducing the bandwidth but keeping the same number of points increases the range limit, but also increases the size of a resolvable range cell.

Resolution in the cross range direction can only be achieved by varying the illumination over the field of view of the sensor system. Figure 7 shows the situation of a sensor system with a wide beamwidth. The sensor sees contributions from all cross range elements that are at the same distance from the sensor. It is possible to resolve objects very precisely in the range direction. However, because the beamwidth of the antenna is large, the cross range location of the object can be anywhere along the constant range arc shown in the figure.

To improve resolution in the cross range direction it is necessary to produce a set of linearly independent observations in the cross range direction sufficient to mathematically solve for the signal contribution of each cross range cell.

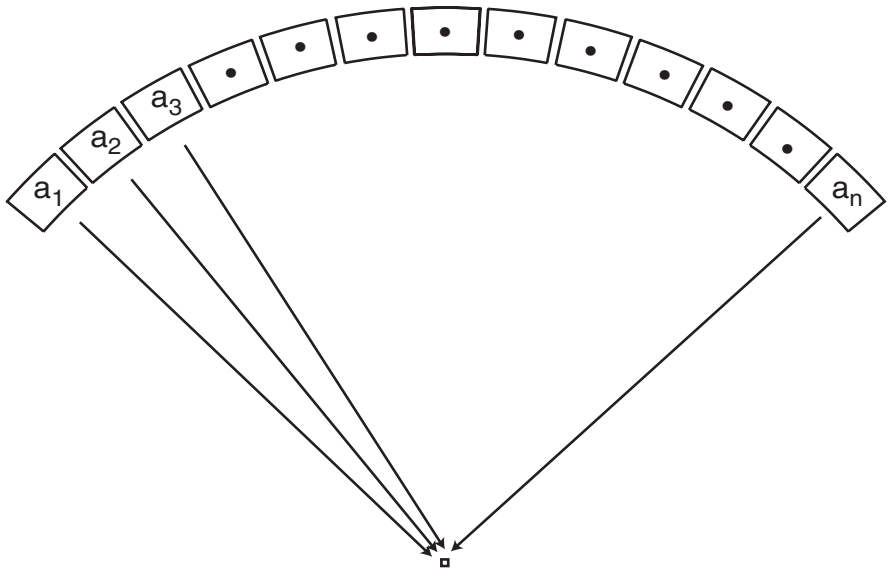

Figure 7 - Each cross range cell contributes to the signal collected at the sensor.

As shown in the figure the rectangular elements, a_n, lie at a constant range from the sensor. For the case shown, these points are all on an arc whose width is the width of the sensor beam pattern. In a stepped frequency radar system, when we transform the frequency sweep to the time domain, each point in time represents a specific distance from the antenna. The signal sensed by the radar is the sum of the signal reflections from each point along the constant distance arc. We can write this in the form of an equation as follows:

$$S(d) = a_1 + a_2 + a_3 + \ldots + a_n \qquad (1)$$

where S(d) is the signal at the distance d and a_n are the reflectivity of each of the points at that distance. Since there are n unknowns, we need at least n equations in order to solve for the individual a_n terms. In order to do this, we introduce a weighting function which comes from the antenna response. This changes the equation to:

$$S(d) = A_1*a_1 + A_2*a_2 + A_3*a_3 + \ldots + A_n*a_n \qquad (2)$$

For the types of radars characteristic of the drawing in Figure 7, each of the weighting elements A_n is equal to one - each cross range element contributes equally to the overall signal return at that range. There are any number of coefficient sets A_n which will allow us to separate the small a terms. Remember that there must be at least n of the sets of A_n. The preferred method of creating this weighting function is by use of a very narrow beam. For the ideal case of an infinitely narrow beam only a single cross range cell is illuminated and the weighting function becomes:

$$A_n(1) = 1\ 0\ 0\ 0\ 0\ 0\ 0\ 0\ 0\ 0\ \ldots 0 \qquad (3)$$
$$A_n(2) = 0\ 1\ 0\ 0\ 0\ 0\ 0\ 0\ 0\ 0\ \ldots 0$$
$$A_n(3) = 0\ 0\ 1\ 0\ 0\ 0\ 0\ 0\ 0\ 0\ \ldots 0$$
$$\ldots\ldots$$
$$A_n(n) = 0\ 0\ 0\ 0\ 0\ 0\ 0\ 0\ 0\ 0\ \ldots\ 1$$

In this case the separation of the equations is trivial. When the antenna beam is not this narrow, more than one cross range element is illuminated at a time and we get a pattern of the form:

$$\text{Real case} \qquad A(n) = 0\ 0\ .25\ .5\ .75\ 1\ .75\ 0.5\ .25\ 0\ 0\ 0\ \ldots \qquad (4)$$

At the frequencies of operation where there is good penetration of building materials, antennas with very narrow beam widths are too large to be practical. The common practice for radar image reconstruction in cases where increasing the size of the antenna is impractical, is to move the radar taking data at various intervals, and then to synthesize an antenna aperture to obtain crossrange resolution.

For peacekeeping and law enforcement applications, while this type of operation is possible, it is operationally less desirable, since there is not always easy access for a vehicle mounted system of this type. In addition, the requirement to detect individuals moving inside a building from a moving platform, as well as doing image reconstruction, makes the processing effort more difficult. This increases the cost of the system. An operationally practical system is one that can be quickly set in place and doesn't require movement or other interaction with the user in order to collect the information for the image reconstruction and motion detection.

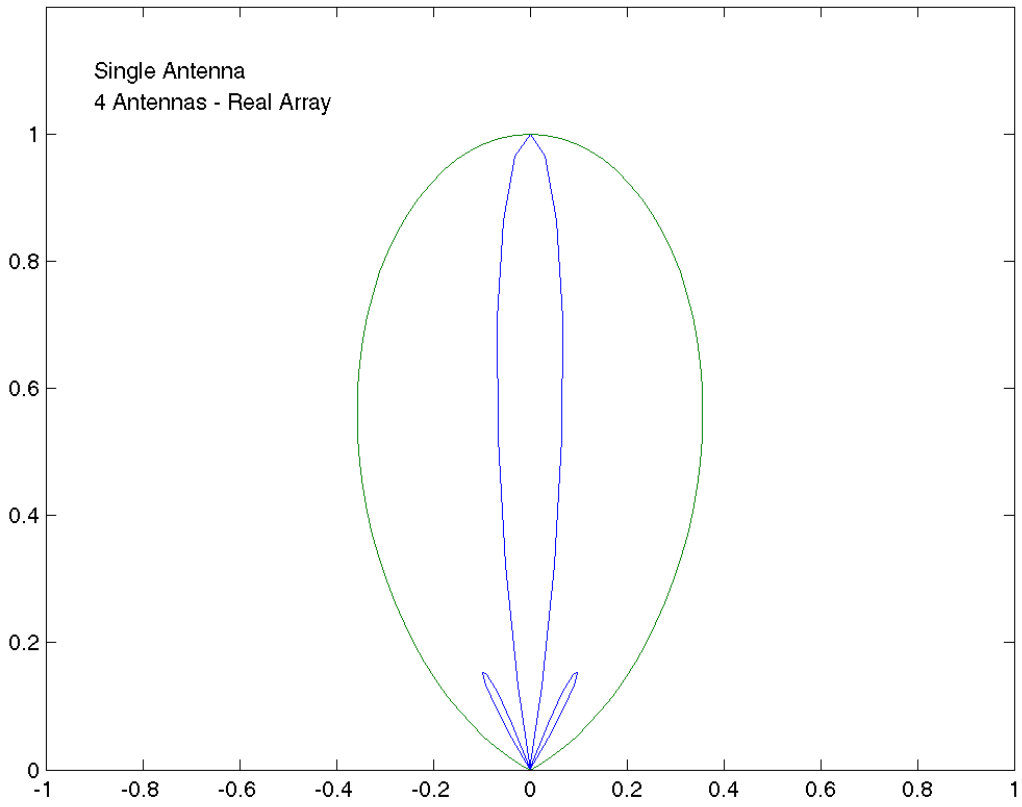

Figure 8 - A multiple element array improves cross range resolution.

Rather than move the radar, it is possible to keep the radar at a single location and synthesize an aperture from an array of antennas. Figure 8 shows a comparison of the antenna patterns of a single antenna, and of a four element real antenna array. The array is made up of antennas with patterns that are the same as that of the single antenna. The decrease in beamwidth achieved with the array is noticeable, and it improves the ability of the system to resolve scatterers in the cross range direction.

An additional improvement in the beamwidth can be achieved by using the same four element array, but scanning the array from end to end. In this case, illumination is provided by transmitting with only a single antenna at a time. The aperture is then synthesized from the resulting data. It is possible to narrow the beamwidth by an additional factor of two, further improving the cross range resolution. Figure 9 shows a comparison of the antenna patterns for a single antenna, four antennas used as a real array, and four antennas used as a synthetic array.

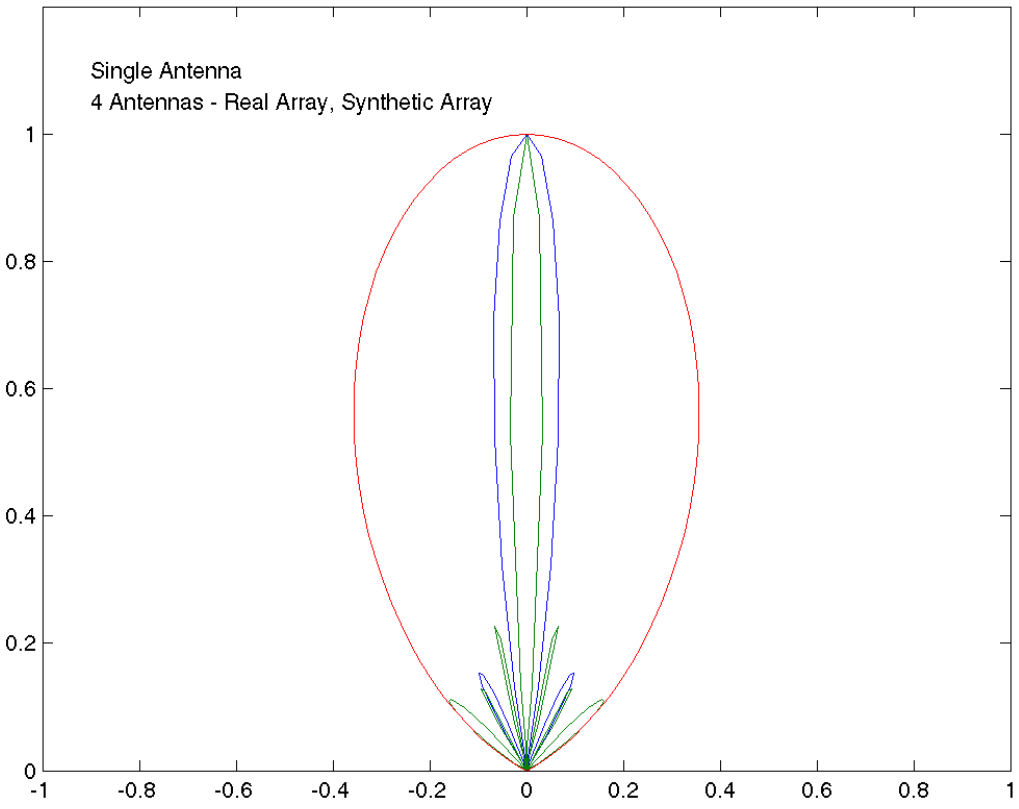

Figure 9 - Scanning a multiple element array improves cross range resolution.

While resolution is constant in the range direction, it degrades with distance in the cross range direction. This is because the width of the antenna beam naturally diverges with distance. The cross range resolution is a function of the wavelength at the lowest operating frequency of the radar, the length of the physical antenna aperture, and the distance to the target being imaged. Figure 10 shows schematically the system parameters that determine cross range resolution of a radar system that scans an antenna array to synthesize an aperture.

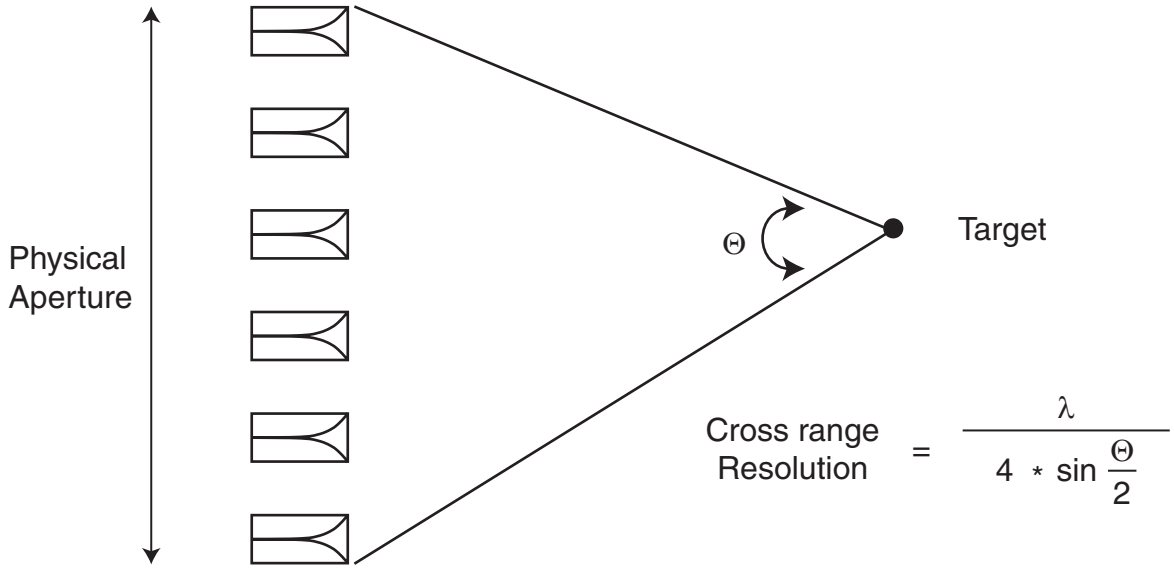

Figure 10 - Cross range resolution of a scanned array radar system.

The cross range resolution calculated with this relation is a measure of how close two targets can be to one another and still be resolved as two targets by the radar. Figure 11 is a table that shows the cross range resolution at a distance of 10 meters as a function of the lowest frequency of operation and the length of the antenna array. As shown in the figure, either doubling the length of the array at a constant frequency of operation, or doubling the lowest operating frequency for a constant length array improves the cross range resolution by a factor of two.

Operating at higher frequencies provides an additional benefit. As shown in Figure 12, the size of each antenna in the array decreases significantly at higher frequencies. A smaller antenna makes an array lighter, more compact, and more easily portable.

Crossrange Resolution
at 10 m - in meters

Frequency (MHz)	Array Length 2.2 m	Array Length 4.4 m	Antenna Height (m)
500	1.37 (53.9")	0.70 (27.6")	0.30 (11.8")
750	0.91 (35.8")	0.46 (18.1")	0.20 (7.9")
1000	0.70 (27.6")	0.35 (13.8")	0.15 (5.9")
1500	0.46 (18.1")	0.23 (9.1")	0.10 (3.9")

Figure 11 - Frequency of operation and array length affect cross range resolution.

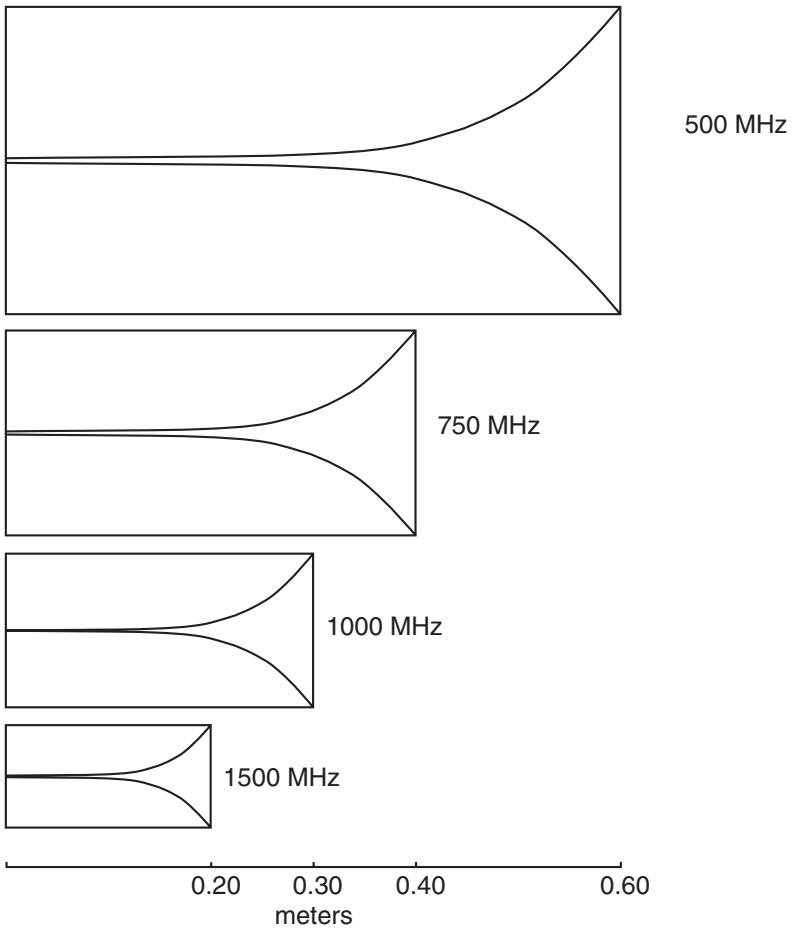

Figure 12 - Antenna size as a function of frequency.

Figure 13 shows experimental confirmation of this predictive equation from data taken for this program. The figure shows a portion of the radar image of a 2.4 m long wall made of wooden studs faced with drywall. The wall is roughly parallel to the boresite of a 1.8 m long antenna array and is approximately 3 meters from the array. For the radar data for this experimental configuration, the lowest operating frequency is 464 MHz. The predicted cross range resolution for this experimental configuration for the nearest end of the wall is 0.606 m. In the image, the first two studs are clearly shown. Measurement of the first stud shows an apparent width of approximately 0.6 meters.

Image reconstruction is accomplished by either of two methods - Fourier transform or backward propagation. Figure 14 (a) shows schematically the Fourier transform method. Taking the Fourier transform of the stepped frequency data for an individual transmit/receive antenna pair

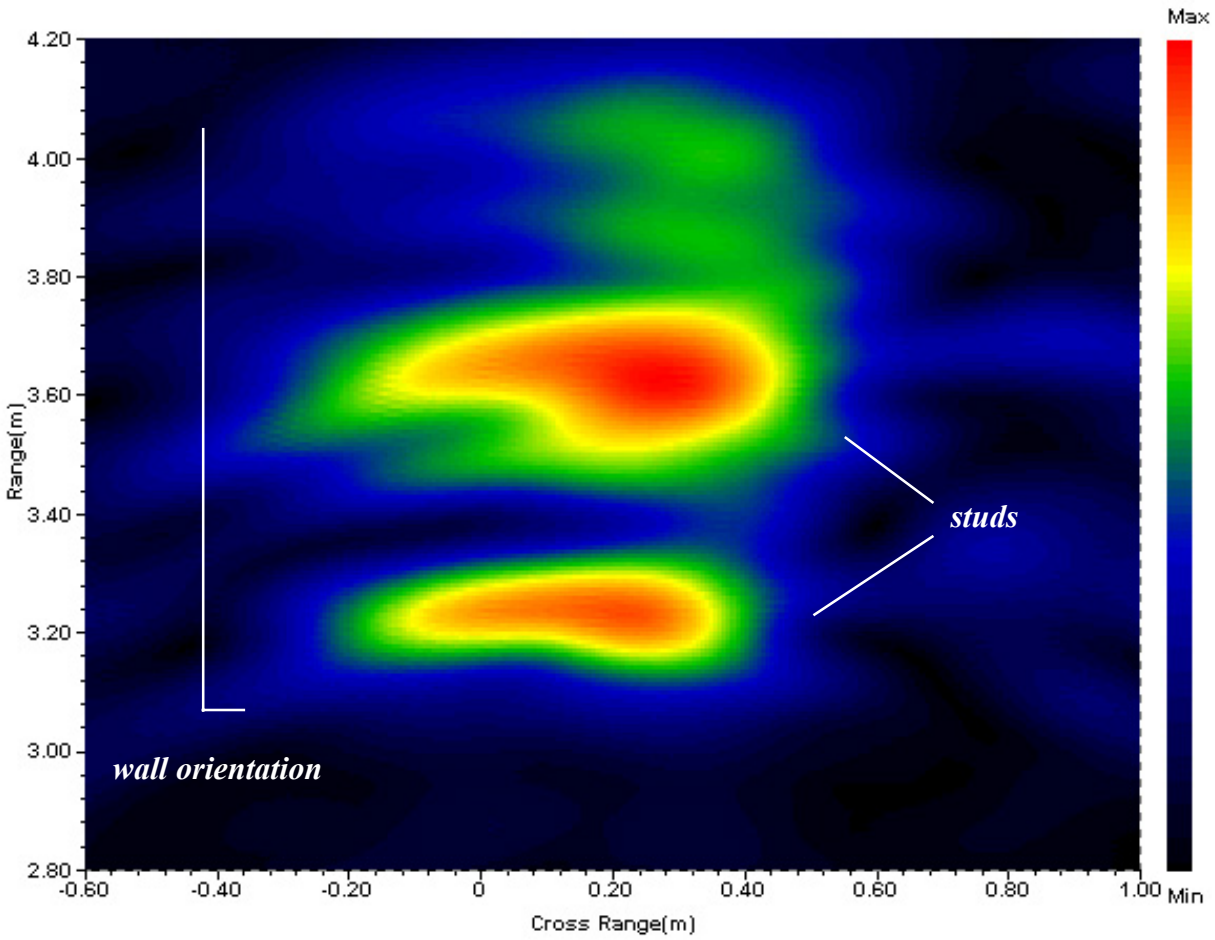

Figure 13 - Image closeup showing two studs from vertical wall.

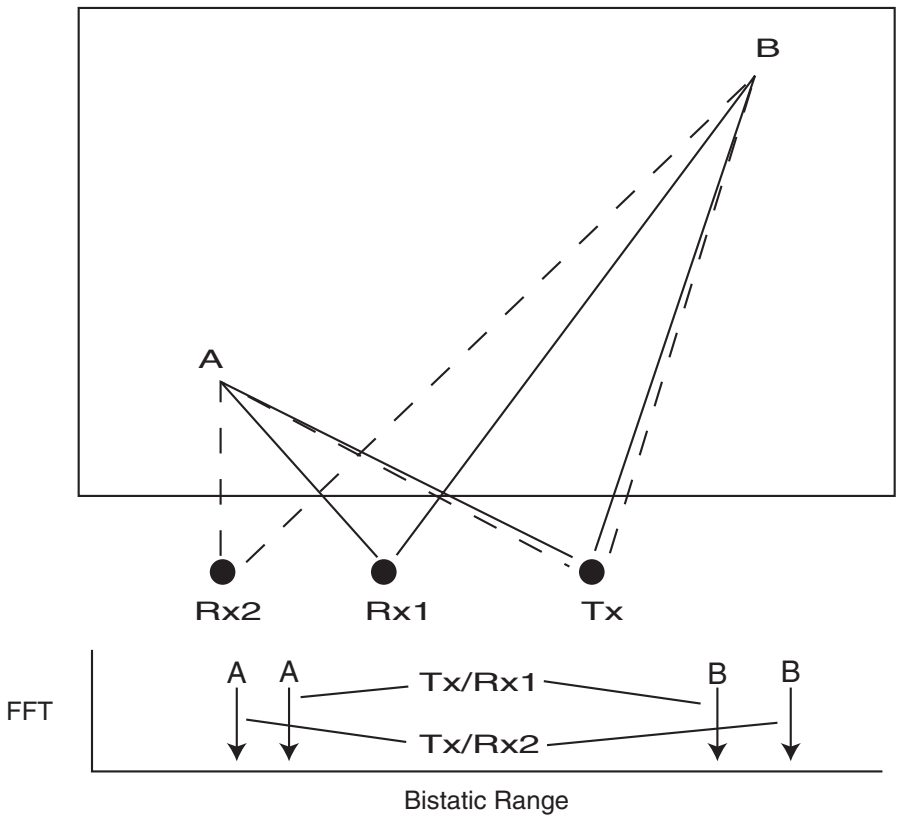

Figure 14 (a) - Image reconstruction using the FFT.

creates a range profile for all of the scatterers in the antenna field of view. The bistatic range to each pixel in the image map is used to index into the range profile to find the value of the in phase and quadrature components of the scattered field from that range. For a different antenna pair, the bistatic range to the same pixel will be different. The values from all of the antenna pairs from the scanned array are summed for each pixel in the image map. Where there are objects in the image that result in scattering, the individual observations from the antennas will be in phase and sum to a large value. Where there are no objects, the individual observations will be out of phase and tend to sum toward zero. The magnitude of the summation depends on the radar cross section of the scattering object and the distance from the antenna array.

The FFT method has the advantage of being relatively fast computationally. Distance weighting can be applied to the result to account for the distance dependence of the magnitude of the electric field, however, frequency dependent effects such as antenna pattern variations can not be accounted for.

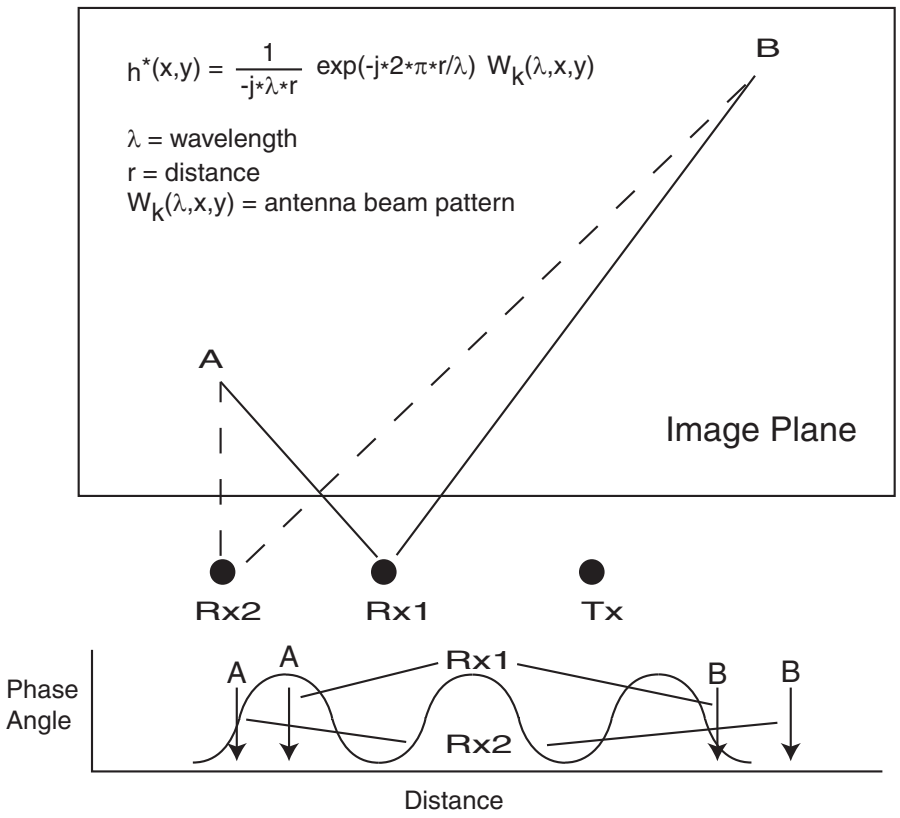

Figure 14 (b) - Image reconstruction using backward propagation.

In the backward propagation methodshown in Figure 14 (b), for each pixel in the image, the data is phase adjusted a single frequency at a time to account for the change in phase associated with the bistatic distance between the transmitter and receiver. During phase adjustment the effects of range attenuation and frequency dependent antenna patterns can be easily included. As in the FFT method, the contributions at each pixel from each antenna pair are summed to create a subimage at each frequency. The final image is formed by summing all of the subimages. In addition to the ease with which corrections for antenna pattern effects can be made, the backward propagation method avoids the necessity of using interpolation as the FFT must do when the bistatic range to a pixel and the FFT range index are not exactly the same. The major disadvantage of the backward propagation method is that it is more computationally intensive.

For cases where there are many objects that scatter energy within the field of view of the antenna array, there will be places in the image map where there will be ghost targets. These targets show up at places where the range profiles of a subset of the antenna pairs intersect. An example is the combination of a multipath return from one antenna pair, coinciding with the direct

path return from another scatterer in the image plane. In these cases, the signal contributions sum, but generally to a lower value than for actual targets. The difference between real and ghost targets will become larger as the signal to noise ratio of the image improves. This can be accomplished by averaging image frames. If Y(n) is the updated full spectrum image, and X(n) is the n^{th} full spectrum image, then Y(n) = (1/n)X(n) + (n-1/n)Y(n-1). An important assumption in applying this scheme is that there are not significant changes from image to image. This updating process is stable and the sensitivity to target motion is not high because the most current image is not weighted heavily. If there are moving targets, they will leave a trail in the image.

Another method for reducing the effect of ghosts is to use additional processing within individual images. Two common techniques are moving average filtering and median filtering. Moving average filters are lowpass filters and will result in trade-offs between resolution and smoothness of the image. A median filter applies a weighting function that varies inversely as the standard deviation of the individual antenna observations at pixels associated with potential targets. Observations for direct path scatterers tend to have very small standard deviations while those for ghosts have a much wider variation. The median filter is not a linear algorithm and is relatively complicated to implement for complex value images.

Motion detection is performed using complete image frames. In its simplest implementation, this is accomplished by subtraction of adjacent images in a sequence. If X(n) is the full-spectrum image sequence, then the 1^{st} order motion detection image Z(n) = X(n) - X(n-1). Higher order detectors are more stable with better signal to noise ratio, but they are less sensitive. The 2^{nd} order motion detection image can be expressed as Z(n) = (0.5)X(n) - X(n-1) + (0.5)X(n-2).

It is possible to superimpose motion profiles on the underlying image. The common approach is to form the display image D(n) = (a)abs[Z(n)] + (1-*a*)abs[Y(n)] where *a* is the parameter, bounded between 0 and 1, that controls the threshold for visualization. Larger *a* emphasizes the changes due to motion with relatively light background profiles. When *a* = 1, only motion is displayed. In order to reduce confusion, it is often the case that color is used to represent the motion term Z(n), and grey scale is used to represent the background image Y(n).

Hardware Development

The brassboard imaging system which we developed consists of three hardware subsystems, 1) the stepped frequency radar, 2) the antenna array, and 3) the radar control and display. In order to reduce program risk, we used a stepped frequency radar that was previously developed for concealed weapons detection under NIJ Grant 97-IJ-CX-K013.

Stepped frequency, CW operation provides advantages over both impulsive time domain and swept frequency operation. Perhaps the biggest advantage is precise waveform control. For through the wall systems, operations will occur in environments where there are other important systems, such as communications and navigation, that operate in portions of the same frequency band. The stepped frequency technique allows complete control over the frequency of emission thereby allowing the radar to avoid transmitting at frequencies where other devices operate.

Another advantage is in the method of narrowband signal reception. Unlike a time domain system receiver which must have a wide bandwidth and substantial gain before reaching the correlator, our radar adds no gain to the system until after conversion to an intermediate frequency. At this point the bandwidth has been reduced substantially giving the receiver good immunity to carrier signals generated by other emitters. A strong carrier anywhere in band for a time domain system is likely to saturate the receiver and result in loss of data.

The radar along with a table of its specific performance parameters is shown in Figure 15. It generates a CW, digitally controlled, stepped frequency waveform over the frequency range of 450 to 2000 MHz, has a power output of 100 mW, and can operate continuously on battery power for 8 hours. Range resolution is controlled by the bandwidth of the stepped CW waveform. Using the full bandwidth allows this radar to achieve a range resolution of approximately 4 inches. As can be seen in the figure, the radar is relatively small, which lends itself to portable applications.

Early program activity was focused on integrating this radar into a data collection system that would allow us to get experimental data for testing imaging algorithms and defining operating parameters for the brassboard imaging system. We set out to build hardware that would allow us to vary the phase and magnitude of the radar signals passed to each antenna, but quickly determined that the experimental system could be simplified by developing a special antenna switch

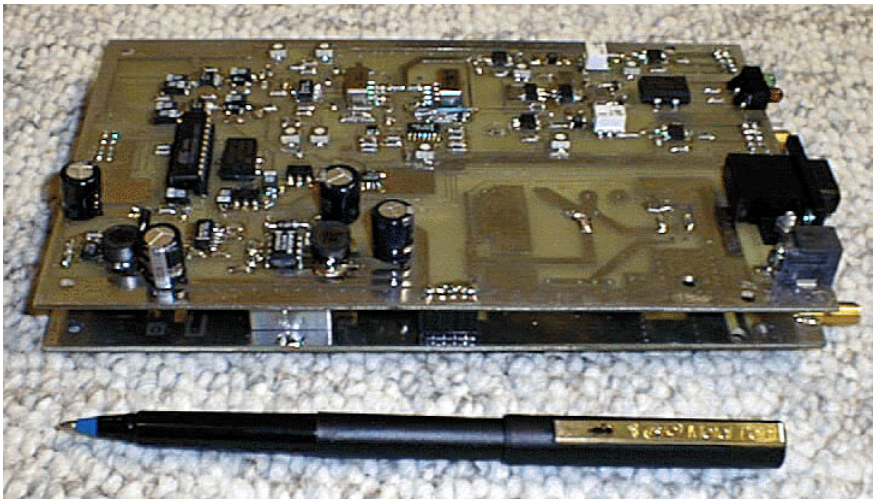

Radar Specifications	
bandwidth	450 - 2000 MHz
range resolution	~4 inches
power output	100 mW
sweep rate	selectable 1 - 8 per second
unaliased range	selectable 45 - 325 feet
size	2" x 6" x 9"
battery	12v, 2.0 Ah
battery life	8 hours

Figure 15 - Stepped frequency radar and performance specifications.

box that would let us select and excite individual transmit/receive antenna pairs with the radar. Since one of the parameters we wished to set through the early experiments was the type of antenna array, the switch box was designed to work with an antenna array that consisted of four separate pairs of transmit and receive antennas (eight total antennas), or with a four element array where each antenna is used to both transmit and receive (not at the same time, however). In addition, the switch box was designed so that two could be connected and up to an eight element array could be used. Figure 16 is a picture of both the radar and the switch box in their final packaged configuration. Each package is approximately 9.5” long, 5.5” wide, and 2.5” tall.

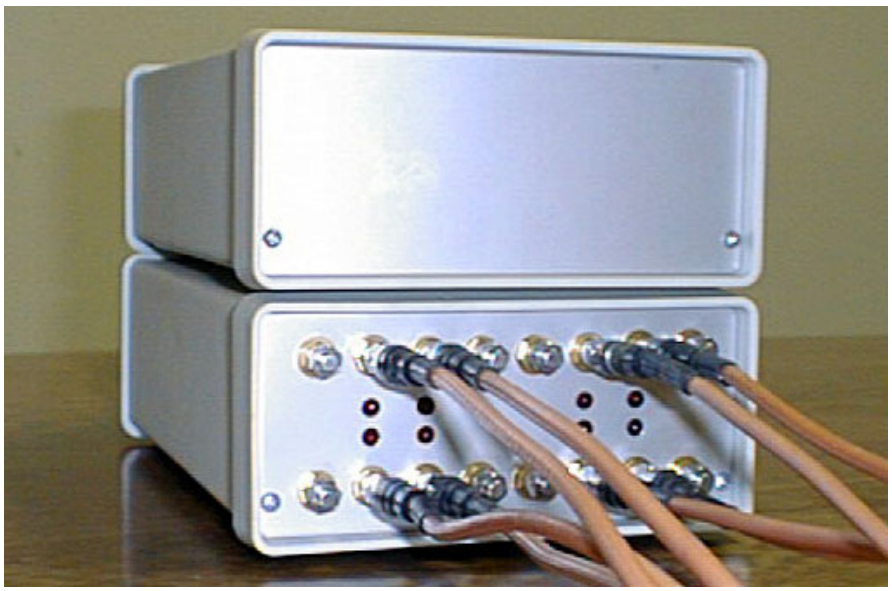

Figure 16 - Packaged radar and antenna array switch box.

Our initial antenna array consisted of 4 pairs of antennas and a mechanical structure that allowed us to vary the spacing between antennas. The antennas themselves were of the Vivaldi design and were fabricated using brass shim stock and plexiglass. Figure 17 shows a photograph of the experimental antenna array.

Figure 17 - Experimental antenna array.

As shown in the figure, the Vivaldi antennas are of the classical design with the tapered slot being formed with two metal plates on the same side of the antenna plexiglass substrate. The antenna feed is a stripline that provides the balanced to unbalanced transition with the radar output. This placed the feed point to the radar on the side and at the bottom of the antenna.

While this method worked reasonably well, the variation in impedance match between the antenna and radar was greater than we desired over the entire bandwidth of the radar. Antenna measurements also indicated that the performance at the highest frequencies was not as good as expected. A contributor to this performance shortfall is the loss characteristics of the plexiglass substrate at the higher frequencies.

As a result, we explored different methods of changing the antenna feed mechanism to improve the impedance match with the radar, and different substrate materials for improving the high frequency performance of the antennas. These methods included making the antennas with the two metal plates on opposing sides of the substrate, using inductive coupling between the plates to provide the impedance transformation and matching mechanism, and using a tapered balun to provide the impedance transformation and matching. Several sets of antennas were made using printed circuit techniques and two different substrate materials. Figure 18 shows two of the antennas fabricated showing the different feed mechanisms and the two sided construction.

Figure 18 - Printed circuit antennas.

Early experiments with the antenna array showed that an array of four antennas separated by 30" gave acceptable image quality. We used this information to embark on the development of a brassboard array. In order to help guide our design activities, we used a draft requirements document provided by the Marine Corps Systems Command that outlined the desired capabilities of a through the wall sensing system that could be used for clearing facilities missions. These requirements helped set our major design goals which were a weight of under 20 lbs, and the ability for a single person to carry, set up, and take down the array.

Meeting these goals required that the array collapse to a size that is manageable. Since the spacing between antennas must be known for the imaging algorithms, controlling the expanding and collapsing characteristics of the array was important. We engaged the services of a consultant with experience in developing lightweight, collapsible structures for satellites. Our discussions with him led to the conceptual design of a collapsible array consisting of rectangular antenna "bays" with diagonal tensioning members to provide stiffness to the array when fully expanded. Each bay consisted of a support frame for two antennas, horizontal arms with hinges and latches to provide repeatable positioning of the antenna frames, and a set of tensioning "wires" to provide the requisite dimensional stability of the bay when fully extended.

A detailed mechanical design of this concept was performed. Because the array is a support structure for the radar antennas, material selection was important. It was decided to use G10, a nonconductive fiber reinforced material, for all of the structural elements. Bids were solicited for array fabrication. We originally were going to fabricate and assemble only a single bay (the whole array consists of 3 bays), but because machining set up costs dominated the cost of the materials, it was decided to fabricate all 3 bays at the same time.

The result of these efforts is shown in Figure 19. When the array is fully expanded it is 2.2 m long (7.2 ft). When collapsed it is approximately 0.28 m (11 in) wide, 0.33 m (13 in) tall, and 0.61 m (24 in) long. It weighs about 17 pounds.

Initial assembly and testing of the array showed that it extended and collapsed very repeatably, although we found that the method of holding the extended arms in place with latches was very cumbersome and slowed down the process of collapsing. In addition, the extension arms were more flexible than anticipated making the array a little less rigid than is necessary for robust use in the field. While we were concerned initially about how the cables linking the antennas and

Figure 19 - Through the wall imaging radar system brassboard.

radar electronics would interact with the folding portions of the array, they did not pose any problem. It was decided that stiffening the extension arms and lengthening them so that they would positively lock against one another, would enable us to stiffen the array and enable us to get rid of the latching mechanisms. We redesigned the extension arms, had a set machined, and reassembled the array. Subsequent testing has shown that these changes have improved the mechanical performance of the brassboard array and make it a good solution for a field test demonstration system.

Our testing showed other characteristics of the array that could be improved, but were considered adequate for the brassboard. These are the overall thickness to which the array will collapse, the weight of the individual antenna support structure, the hinge mechanisms on the extension arms, and the overall simplicity of the folding mechanism. Because there was insufficient level of effort to perform another complete design, we did some quick prototyping of two different concepts, one that uses different hinge mechanisms, and one that uses a different antenna mounting structure with smaller antennas.

The brassboard array and the small antenna array have been used in an extensive set of tests. These experiments have given us insight into areas where sensor performance needs to be improved. In an attempt to determine whether the antenna array could be reduced in size, one set of radar electronics was modified to extend the upper frequency limit to 3000 MHz and used with the prototype small antenna array. By extending the upper frequency of operation, we were able to operate the radar at a higher lower frequency limit using smaller antennas while maintaining the same bandwidth, and therefore, range resolution.

A second area identified for improvement is the coupling response between the antennas. The largest signal received by the sensor is the direct path signal between a transmit and receive antenna pair that are adjacent to one another in the antenna array. Sensitivity of the radar receiver must be adjusted so that it does not saturate from this direct path signal. As a consequence, the minimum detectable signal for the sensor array is set by this condition. The minimum detectable signal value determines the practical operational range of the sensor. Lowering this threshold will increase the effective range, or allow for greater penetration through more highly attenuating wall materials.

The direct path coupling between antennas can be reduced either geometrically through increasing the physical separation between antennas, or by active methods. Increasing separation makes the antenna array longer and increases the size and weight of the system. Doubling the distance between the antennas, however, will only reduce the antenna coupling by 6 dB. The active method consists of electronically cancelling the direct path signal by sampling the transmit signal, inverting its phase and magnitude, and adding it to the received signal. Such a technique is commonly used in narrow band systems with good success. Broadband cancellation techniques are more difficult to implement.

As part of our experimental activities we breadboarded an active cancellation circuit to determine both the degree of difficulty, and the likelihood of success of using this technique to improve the performance of our radar system. Figure 20 is a photograph of the active cancellation circuit breadboard. Figure 21 shows the frequency plots of two wideband radar sweeps (464 - 2000 MHz) where one has had the antenna direct path actively cancelled using this breadboard circuit. As can be seen in the figure, we have been able to achieve between 20 and 25 dB of cancellation

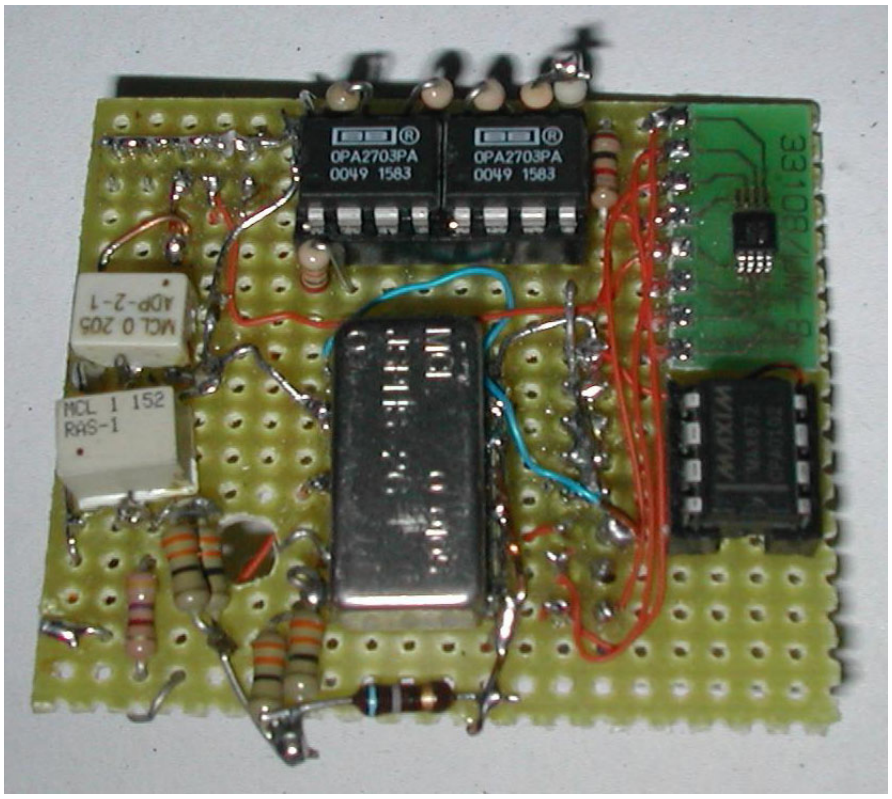

Figure 20 - Active cancellation circuit breadboard.

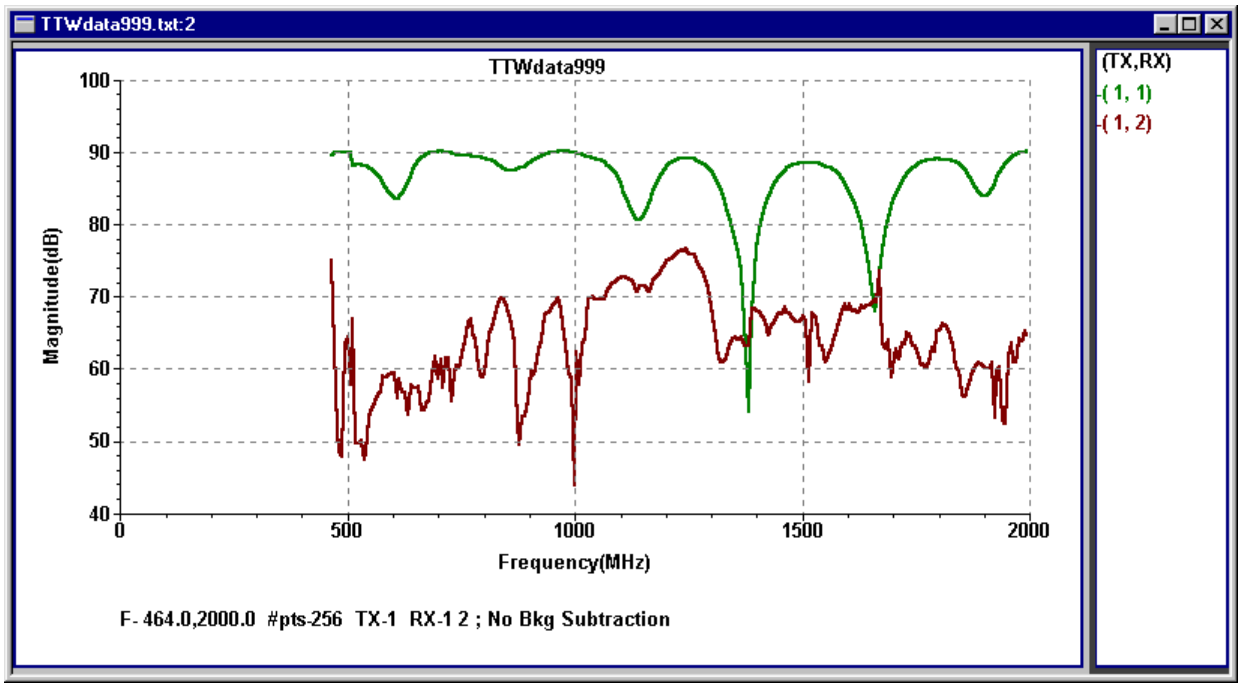

Figure 21 - Active cancellation improves antenna coupling response.

using this method. To achieve the same isolation geometrically would require separating the antennas by 40 feet. Incorporating the cancellation circuit in the radar would have required a redesign. This was not within the program scope so no further investigation was pursued.

A final area identified for improvement is the sweep speed of the radar. Our testing showed that the imaging system will track the motion of individuals behind walls, but it can't do so at a fast enough rate to be operationally practical with the current radar electronics. In addition, we can't average enough frames to increase the signal to noise ratio and improve image quality.

As part of our breadboard activities, we identified, ordered, and tested the performance of a direct digital synthesizer chip from Analog Devices. Using direct digital synthesis to generate the radar frequency sweep would increase the sweep speed of the radar, allow selection of frequencies anywhere within the band of interest without being constrained by a frequency step size, and generate the frequencies with a much lower level of phase noise. Tests of the synthesizer chip verified these performance characteristics, however, trying to use the chip to generate the frequencies required for our system directly, results in a level of power consumption that is too high for a portable system.

We performed some conceptual design, in cooperation with another contract, on a sweep generation method using the synthesizer as the local oscillator for a phase lock loop controlling a higher frequency voltage controlled oscillator. We found that it is possible to retain the benefits of the synthesizer while running it at lower power consumption levels. The resulting sweep speed would be fast enough that the radar would be able to generate complete images at video frame rates. Incorporating this capability in the radar would require a complete redesign which was not within the scope of the program. As a result, no further activity was pursued in this area.

Software Development

The software which was developed for the program evolved to support program needs. We developed a set of software programs integrated into an environment that made it easy to both collect and process data with the experimental and brassboard test systems. These programs were accessed through a windowed interface that allowed us to both control hardware data collection and view processed results interactively. This interactivity allowed us to change test parameters, view results, and make judgements about how to change test parameters to investigate phenomena observed during the testing process. Since it wasn't clear at the beginning of the test program what types of data analysis would be necessary, the structure of the software had to be flexible enough to allow easy addition of different analysis methods suggested by the test data.

Signal processing and data acquisition and control algorithm development were separated initially. All signal processing algorithm experimentation was performed using MATLAB. This allowed us to quickly explore the trade-offs associated with the number and spacing of antennas in the imaging array, build and debug algorithms for image reconstruction, and generate simulated data that could be used to test the image formation algorithms. We formed a collaboration with Dr. Hua Lee of the University of California, Santa Barbara (UCSB), who is a recognized expert in the field of tomographic image reconstruction. Dr. Lee guided our development efforts in the area of the image formation and motion detection algorithms.

Data acquisition and control software development began using the LabView for Windows software from National Instruments. This software was selected since it provides a visual development environment tailored for the control of laboratory instruments. Since we had decided to use a single radar with a sequentially scanned antenna array, the initial development focused on

identifying and implementing the structure for controlling and debugging radar performance. Because we used an existing radar, most of the control functions could be tested as they were developed. Provisions were made to allow user control over the method and sequence of scanning the antenna array. The interface that was developed is shown in Figure 22.

For the radar, the start and end frequencies of the sweep and the number of frequency points in the sweep were the major variables. Selecting the number of sweeps and scans to average allowed us to build up higher signal to noise ratio data. A scan is a complete set of frequency sweep data for all of the antenna combinations.

For the antenna array, we made provisions for scanning either in a pairs or linear mode, and within each mode selecting the combinations of antennas desired. In pairs mode, the array has separate transmit and receive antennas. With a four element array (four pairs of antennas) there are 16 transmit/receive antenna combinations. In linear mode, the array has only a single set of antennas, with one at a time being used to transmit while the others receive. With a four element

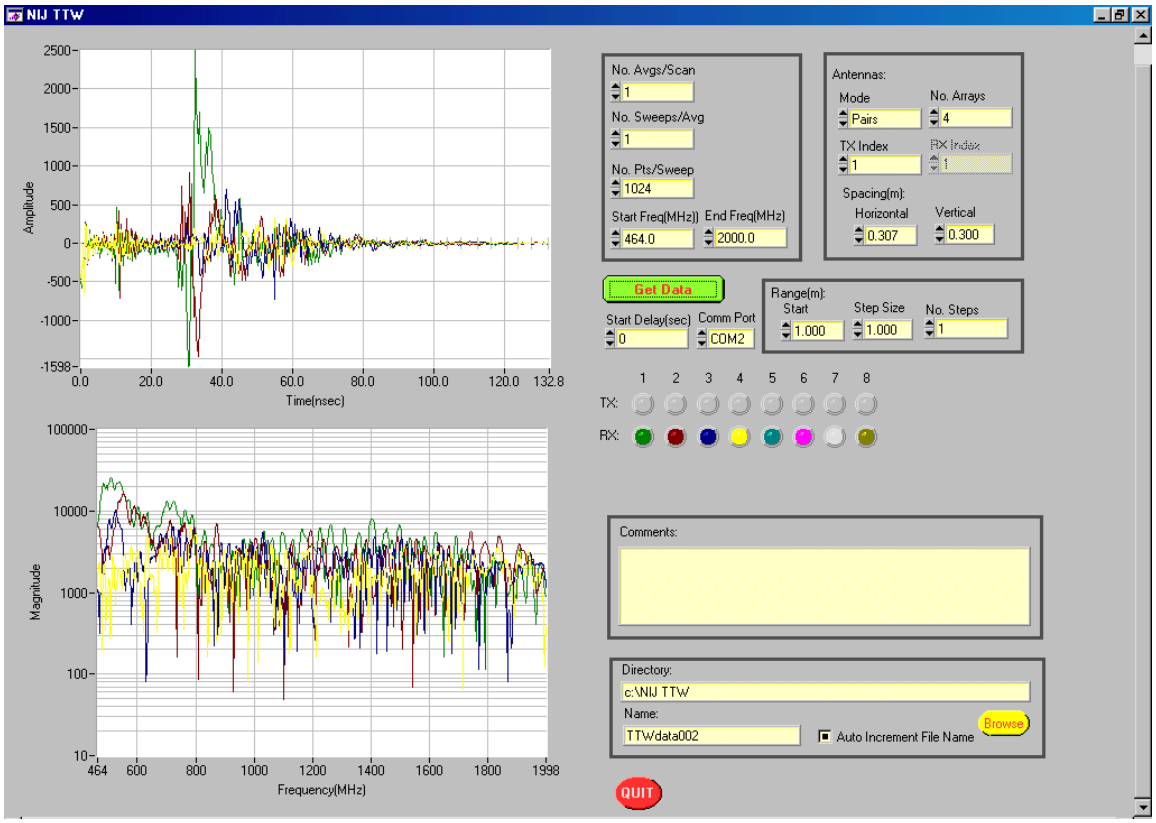

Figure 22 - Initial LabView interface for radar control.

array of this type there are 12 transmit/receive combinations. For both cases the user specified both the horizontal and vertical spacing of the antennas. This information was embedded into the header of each data file and used by the signal processing algorithms during image reconstruction

Charts showing both the time and frequency domain response were added in order to help with debugging hardware performance. By looking at the frequency domain representation of the data it was easy to determine whether adjacent antennas were so close that the radar receiver began to saturate, whether the gains of individual channels of the array were well matched, and whether there were problems with any of the connecting cables.

Since LabView was designed for ease of use and control primarily of laboratory instruments, it runs as an interpreter. We found experimentally that the speed was insufficient to keep up with the rate at which the radar would operate. As a result, we turned to the LabWindows program which allowed us to compile the LabView resource elements and write more efficient programs in C++ to implement the control and display functions. While this improved the speed of operation, we ultimately found that the LabWindows graphical display functions would not support the image reconstruction and motion detection algorithm requirements.

At this point we began the process of implementing the interface in Visual C++ using the Microsoft Foundation Class (MFC) library. The Multiple Document Interface(MDI) was chosen because it enables the simultaneous display of results (plots, tables, etc.) from more than one data source (files, data streams, user input, etc.). The MDI employs a Document/View architecture. A Document is an object that is typically responsible for collecting, manipulating, and storing data. Each Document object type may have one or more View object types associated with it, and these objects may be displayed as the program sees fit. Each View object embodies a visual presentation (plots, tables, forms, etc.) of some or all of the data from the associated Document object, i.e. it typically controls a window whose contents are a representation of the data.

A commercial graphics library, the Graphics Class Library for MFC, from Quinn-Curtis, Inc. was used to handle most of the plotting tasks. In order to deal with a few problems that could not be handled by the standard version of the library, modifications were made using source code purchased from the manufacturer.

The Document/View architecture, the functions available from the Quinn-Curtis library and the procedures dictated by it, and the event-driven nature of Windows all affected choices made in the design of the software.

Figure 23 shows the resulting user interface. The four major functions of the program are accessed from the File, View, and Tools menus at the top of the main window. These functions are acquisition of single image frames, acquisition of sets of image frames that can be used for motion detection studies, definition of the low level signal processing parameters that are applied to the image and motion detection algorithms, and display and manipulation of the raw data collected from the radar. When the desired function is selected from one of the menus, the program launches a form that allows the user to specify the appropriate control parameters and then start the selected task. Figure 24 shows the data acquisition function selection form.

This form is where the operating parameters of the radar are specified before the beginning of any test series. The user can select the start and stop frequencies of each sweep, the number of

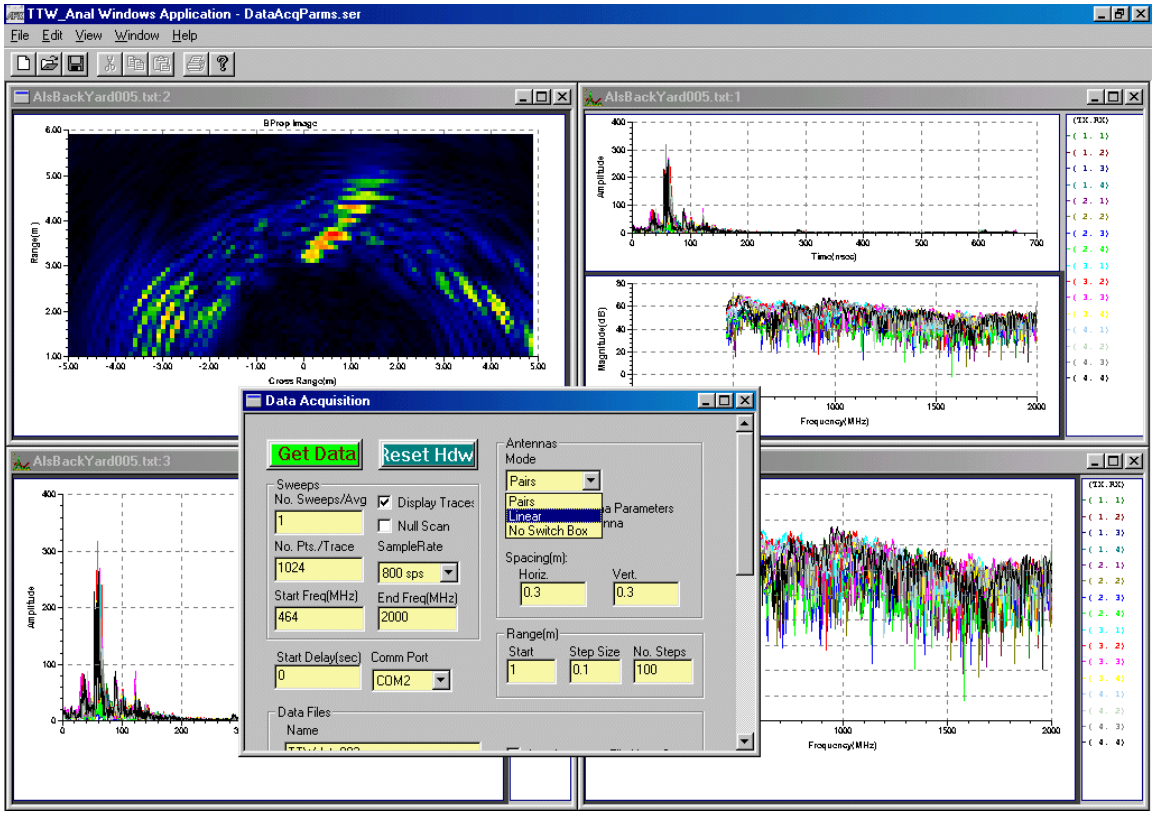

Figure 23 - Final interface for radar control.

frequency points for each sweep, and the sample rate per frequency point. While the user may select arbitrary frequency ranges and numbers of points, the physical limits of the radar impose some restrictions. The software will adjust these selections so that they are physically realizable by the radar. For example, the spacing between frequency points is limited to multiples of 0.25 MHz by the hardware design of the radar. Based on the frequency range desired and the number of points specified, the software will adjust the number of points by using the frequency step size that gives the number of steps closest to that specified over the selected frequency band.

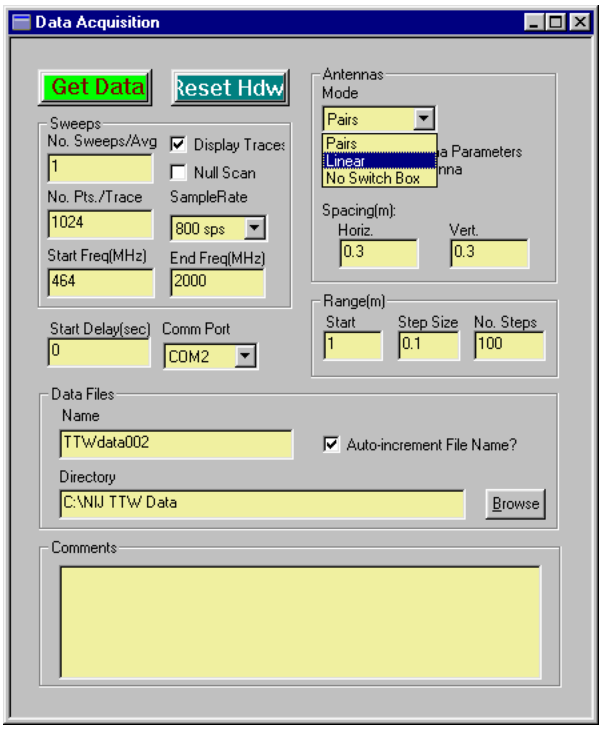

Figure 24 - Data acquisition selection form.

Other parameters that may be selected are the number of sweeps to average while taking data (to build up a higher signal to noise ratio data set), whether to display the data graphically as it is being collected, the name to give the resulting data file, the directory path where the data file is to be stored, whether to automatically increment the file name for subsequent tests, and which serial port to use for communication. While the communication with the radar is all through the serial interface, this is not the element of the system that limits the speed of data acquisition. Maximum sweep speed (samples per second) is determined by the settling time of the hardware frequency generation circuit within the radar.

There are three different modes of operation that can be selected for the antenna array. In linear mode, there is a single set of antennas where each antenna is sequentially used as a transmitter while the remainder are used as receivers. In pairs mode, there are two sets of antennas with one set being dedicated transmit antennas and the other set receive antennas. The no switchbox mode allows testing of a single pair of antennas. This is useful for performing direct path measurements and characterizing antenna response where it may be desired to use antennas that are not physically part of the imaging array. It is important to note that the user can additionally select subsets of antennas in the array to use for data acquisition. However, this specification is entered through the Analysis Parameters form.

After specifying these parameters, the user must only press the get data button on the form to begin data collection. The radar then performs the required tasks and sends back the data where it is displayed on the computer and saved to a disk file. Antenna spacing and range parameters are saved as file header information and present for file compatibility with a backward propagation algorithm developed by our UCSB collaborators. Figure 25 shows the display interface at the conclusion of data acquisition. The top graph shows amplitude vs. time while the bottom graph shows magnitude vs. frequency for each antenna pair. At the bottom of each graph is a text field that shows what frequency range, number of points, and antenna combinations were specified. If the user has selected the display trace option for data acquisition, then each of the individual traces is displayed on the screen as it is collected.

At this point the user may choose to view the data in various ways. This is accomplished through using the View menu or by placing the mouse cursor anywhere within the plot area and

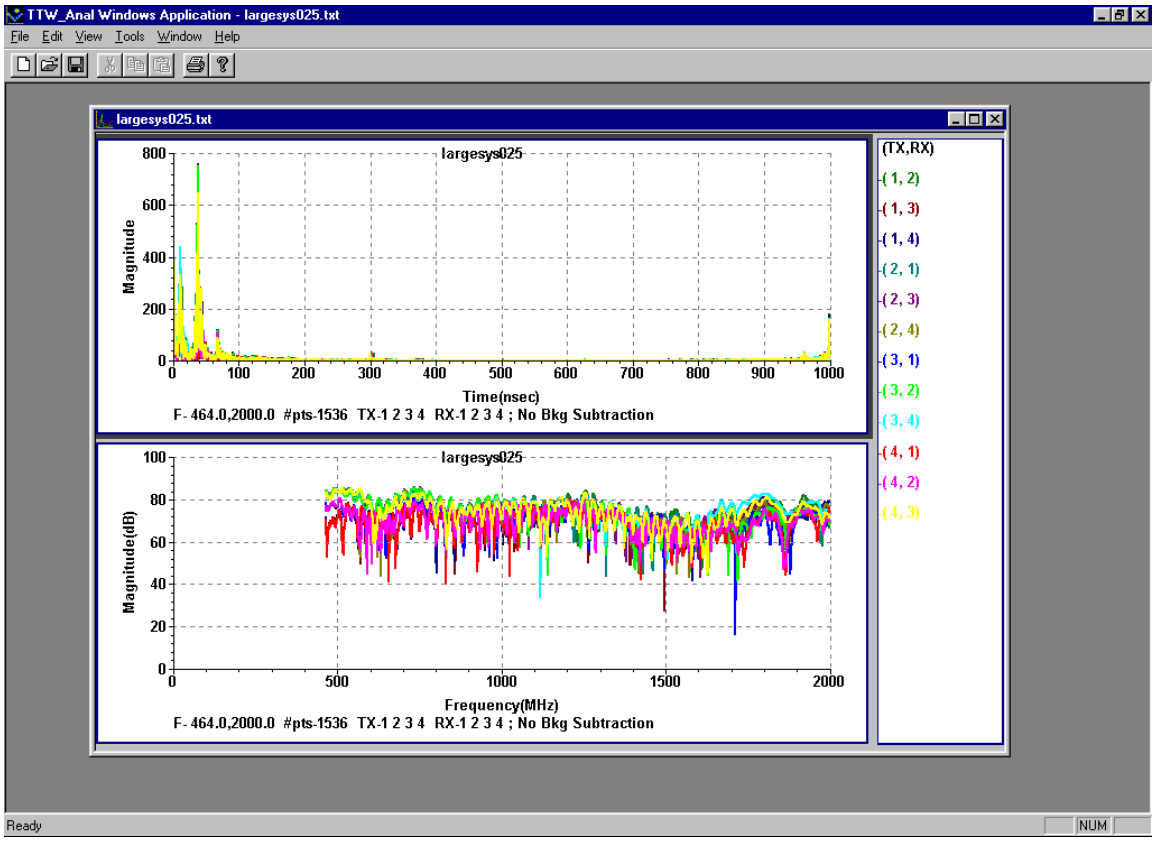

Figure 25 - Data acquisiton screen display.

single clicking the right mouse button. This action produces a flyout menu with the various options for viewing the data. Figure 26 shows the flyout menu and the selections available. The basic data view shows both the time and frequency domain representation simultaneously. Using the options from the flyout menu the user may create individual views of the data that can be manipulated separately and compared to one another. As seen in the figure the options include individual time and frequency domain plots, three different representations of images, methods of viewing the raw data, and ways to view subsets of the data and cross plot individual data traces from more than one test.

Each plot may be changed individually. There is a zoom function provided for examining different parts of the plots and images in more detail. This is accomplished by placing the cursor in the plot area and holding down the left mouse button while dragging a selection box around the area for which a more detailed view is desired. The software automatically rescales and replots the data. This action can be undone by selecting the Unzoom option from the flyout

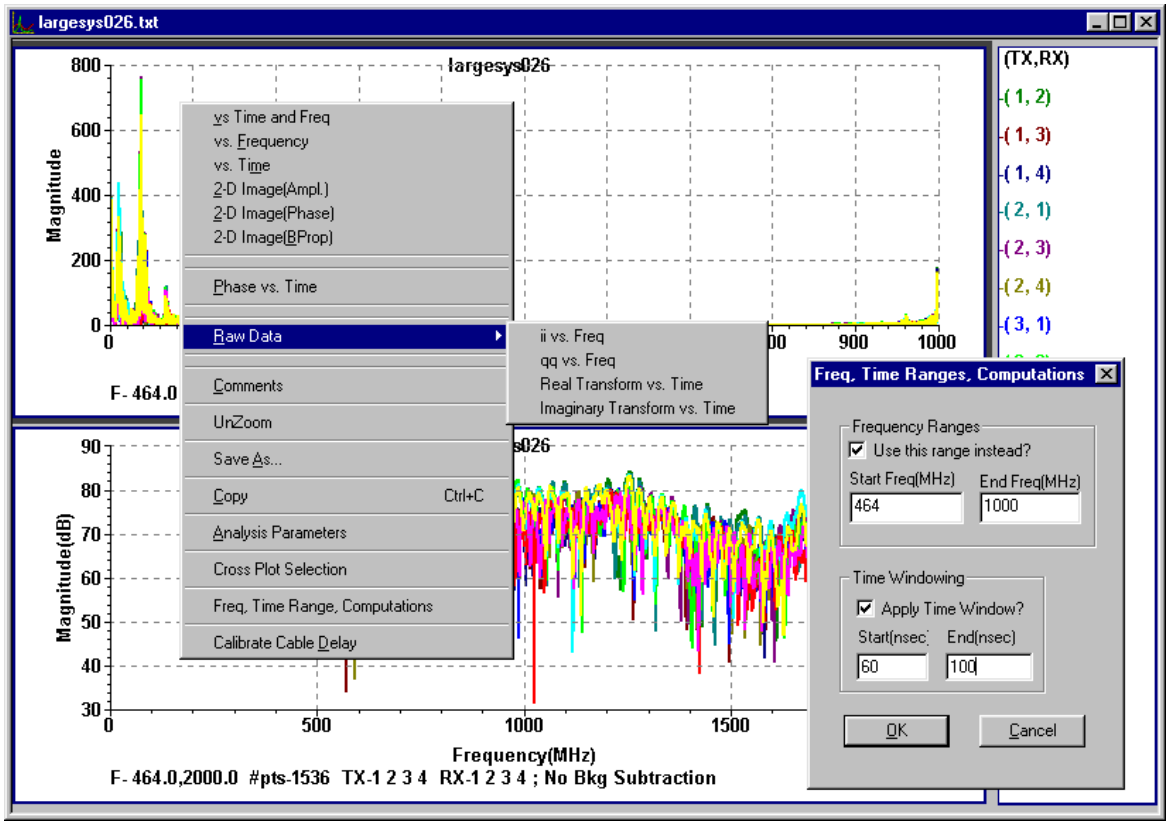

Figure 26 - Data viewing options.

menu. In some cases, however, the automatic scale selection may be different than what the user desires. Alternatively, the plot axes can be manipulated individually by the user by placing the cursor on the axis and double right clicking. This brings up a form that gives the user control over the scale, grid, line attributes, and axis extent.

The frequency band selection option is particularly useful since it allows the user to investigate the interaction between image quality and radar operating parameter selection. As an example, consider the three images shown in Figure 27. Each image is formed using the same data set which is from a test where a person is standing at a distance of 10 meters from the imaging array and behind an interior wall that is 4.6 meters in front of the array. The wall extends horizontally from 0 meters to 2.4 meters.

In the first image, the entire frequency band between 464 and 2000 MHz is used to form the image. The person is clearly seen beyond the wall as are two of the supporting wooden members of the wall. In the second image, only the frequency range between 464 and 1000 MHz is used to form the image. The person is still seen strongly but the smaller wooden support features are not. In the third image, the frequencies between 1000 and 2000 MHz are used to form the image. For this case, the person disappears but the features of the wall begin to show up more sharply. Being able to interactively examine the data in this manner has proven to be very useful in helping to define the features an operational imaging system might require.

The Analysis Parameters option gives the user a different set of parameters that can be selected for manipulating and viewing the data acquired with the radar. Selecting this option either from the flyout or View menu creates a form with multiple tabs from which a range of radar and plot functions can be specified and changed. Figure 28 shows a composite view of the parameter selection tabs. The center image in the figure shows the entire Analysis Parameters form. There are three buttons on the bottom of the form for saving a set of analysis parameters, loading a previously saved set of parameters, and applying any changes made to the options in the various tabs to all subsequent data views. The default tab allows the user to specify data files to be used for background subtraction or data normalization.

The antennas tab is very important. Only the antennas that are selected in this tab are used during data acquisition. For a file that has previously been acquired using all of the antennas, checking or unchecking these boxes will determine whether data will be displayed when select-

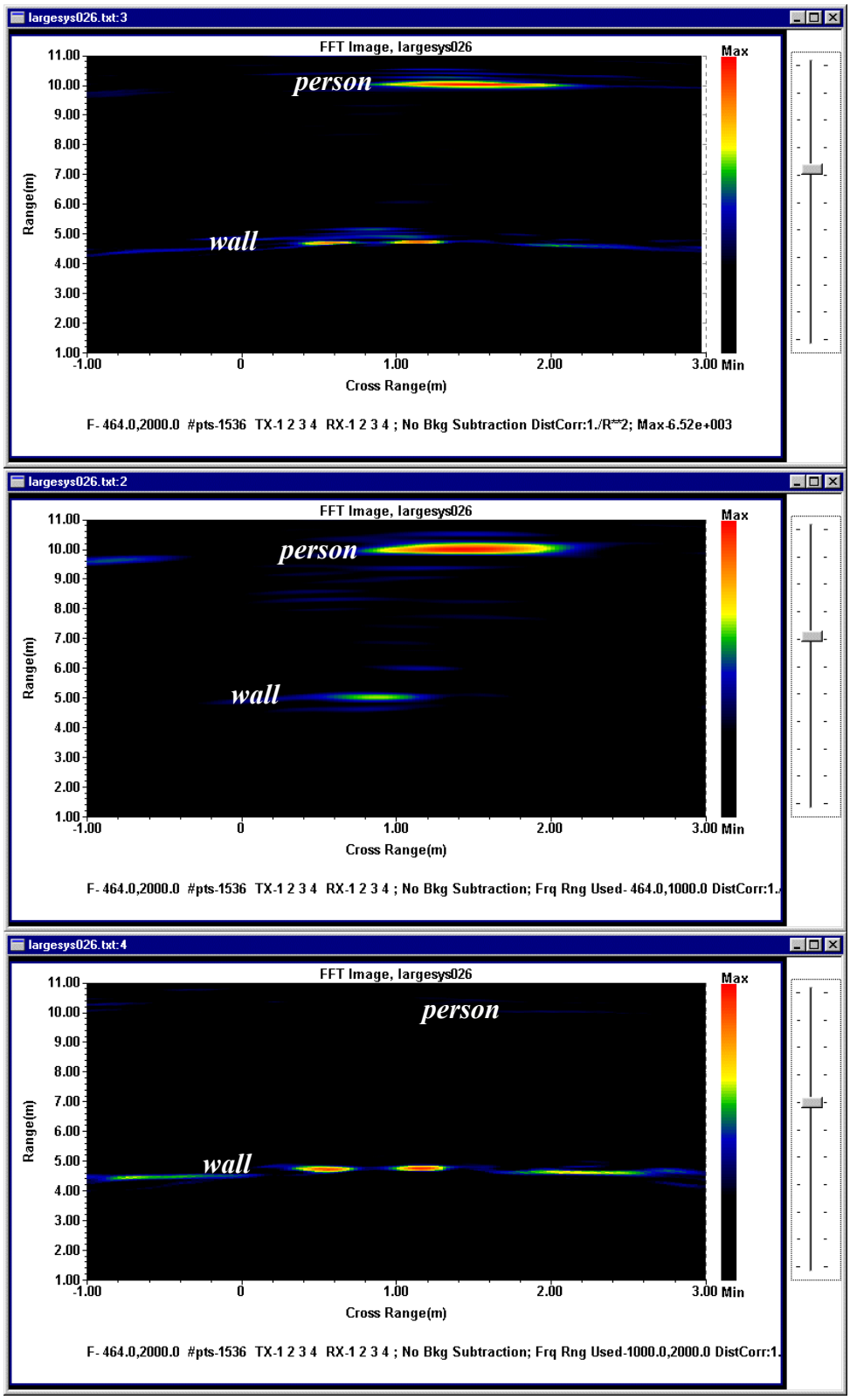

Figure 27 - Effect of frequency band selection on image quality.

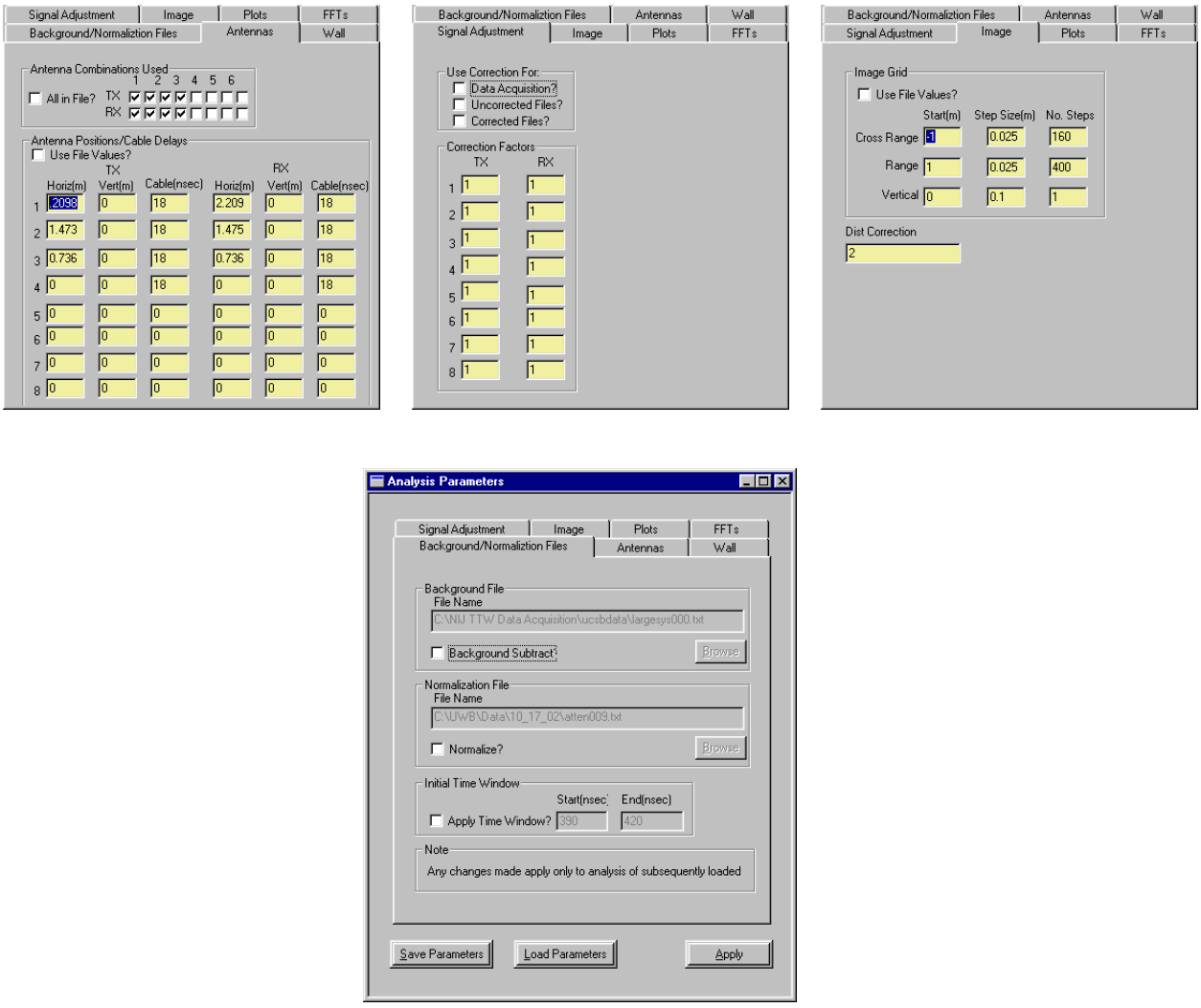

Figure 28 - Analysis parameter selection options.

ing the various data viewing options. The portion of the form for specifying antenna positions and cable delays must be accurately filled in since the image formation algorithms use these values. If they are incorrect, the image formation will fail.

The signal adjustment tab is for making adjustments to the individual transmit and receive channels to make up for differences in gain associated with each channel. Occasionally during testing it is discovered that a portion of the imaging array is performing more poorly than the other elements. This can be caused by something as simple as a cable connector becoming loose and causing a higher attenuation path. By using the signal adjustment tab, this change in attenuation can be compensated for numerically. In general practice, the values for these correction factors should be 1.

In the image tab, the user controls the parameters of the image reconstruction displayed. Values for range, cross range, and vertical dimensions are specified by selecting the origin for reconstruction and then the values for the image grid spacing and the total number of image grid points. All these values are relative to the values specified for the location of the antennas in the imaging array in the antennas tab of the analysis parameters form. The distance correction parameter is to allow the user to apply a distance weighting function to the data. This number is an exponent of the distance and generally varies between 2 and 4.

The fft tab controls the number of points the software will use in calculating the range profiles from each transmit/receive antenna pair. If a value greater than the actual number of data points is selected, the fft will be constructed using zero filling. What this does is provide a mathematically correct method of interpolating between points in the collected data and smooths the image.

The plots tab applies only to the raw data display graphs. It is used to control the thickness of the lines plotted on the screen and to specify whether the magnitude or the real part of the fft is plotted for the time domain representation.

Finally, the wall tab allows the user to explore the effect on image reconstruction of walls of different types. Since the speed of light in a dielectric material is slower than in air, a thick wall will distort the reconstruction of an image of objects behind the wall. While the difference in dielectric constant between air and the wall will also cause refraction, we have ignored this effect in our image reconstruction calculations. We assume that the imaging array is parallel to the

wall and have the user select the distance from the array to the wall, the dielectric constant of the wall, and the thickness of the wall. There is no provision to allow the dielectric constant to vary with frequency.

The Image Acquisition function is designed to allow the radar to collect data continuously so that motion detection algorithms can be tested and compared. This function is accessed from the File menu and when selected creates an Image Acquisition form with multiple tabs, as shown in the composite view of Figure 29, from which image acquisition and analysis parameters can be specified and modified. The center image in the figure shows the entire Image Acquisition form with the default get data tab selected. From this tab the user can save and load previously stored settings from the entire form, select the type of motion detection algorithm to use for displaying the data as it is being collected or played back, select whether to get data from the radar or a file of previously stored test, set the record or playback process to pause after a set number of scans or at the completion of a sweep for a specific transmit/receive antenna pair, and playback a stored data file from a specific point in time. Once started, image acquisition proceeds until either the pause or the stop button are pressed.

Of the six remaining tabs, the antennas and wall tabs are identical to those found in the Analysis Parameters function. However, in order to keep static imaging analysis separate from motion detection analysis, the parameters for these tabs must be entered separately.

Control over the radar parameters is from the data tab. The user may select the number of points per sweep, the sweep sample rate, and the starting and ending frequencies for the sweep. As for the static imaging Data Acquisition function, the software will internally adjust the radar's physical parameters to the closest values specified by the user.

The background image and motion image tabs are similar. These two tabs allow the user to see the static background image in grey scale with the motion detection image in color. The background image tab is used to specify the dimensions of the image map and the number of points to use when forming the range profiles from each antenna pair. The motion image tab is used to specify the type of motion detection algorithm and display characteristics. Both tabs have provisions for applying distance correction weighting and frequency band editing so that these parameters can be set independently for each. These modifications are applied in the same manner as described for the Analysis Parameters form.

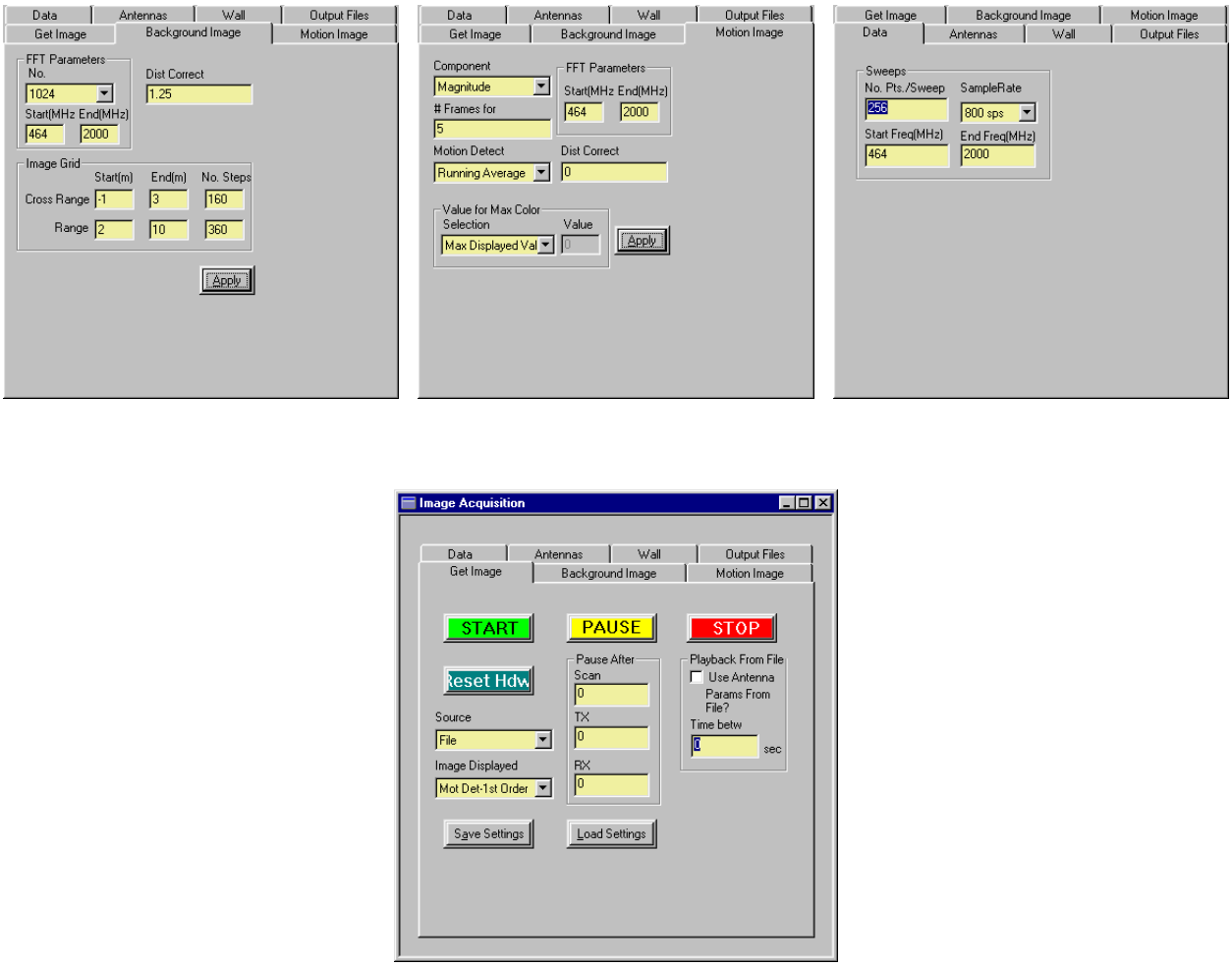

Figure 29 - Image acquisition parameter selection options.

The output files tab allows the user to specify whether to save the motion detection data to a file and provides fields for naming the data files and directory to which they should be stored.

Our software development activities were aimed primarily at creating a testbed for exploring various image and data analysis functions, so optimizing algorithm performance for speed of execution was not addressed. Motion detection performance was limited by the sweep speed of the radar. However, our hardware conceptual design activities indicated that it is possible to build a radar that will provide sweeps speeds high enough that we will be able to collect data at up to 30 image frames per second. With this rate of data acquisition, the efficiency of the image and data analysis becomes a concern.

To get some idea of how difficult the image processing task would be for an improved radar system, we modified the control and display software and ran a series of benchmarks so that we could identify processing bottlenecks. Measurements for data acquisition, data correction, data transformation, image formation, detection algorithm calculation, and image display times were made. While none of the code has been optimized for speed, we found that the image frames can be created once every 0.8 seconds for an image that is 320 x 240 pixels. As indicated above, for our concept radar design we will be able to take data at a rate that will support image frame rates of 10 to 30 per second. This means that the signal processing speed must be increased between a factor of 8 and 24 in order to operate the radar in real time. We have already identified algorithmic changes that will increase the speed of processing, but it is likely that a combination of specialized hardware and additional algorithm optimization will be necessary.

While the variety of features that have been implemented in this control and display software is significantly greater than would be necessary for an operational system, it has given us the opportunity to explore the effects of various algorithms and radar characteristics for their effect on system performance. This software test bed refined our understanding of the real world algorithm and hardware issues that need to be considered for further sensor development.

Experimental Analysis

Experimental testing was performed in support of algorithm development and sensor performance analysis during the program. The earliest set of tests were performed using an experimental eight antenna element array. Our primary objective for this set of tests was to assemble a set

of data that could be used to test both the backpropagation and fft image reconstruction algorithms. A set of three 2.4 m x 2.4 m (8' x 8') stud walls covered on one side with drywall were made and used in various configurations for the tests.

Our simulation activities had us concerned that we would be unable to see walls that were perpendicular to the boresite of the antenna array, so we tested this configuration with a single wall. Other test configurations included a single wall at a 45° angle, two walls forming a 90° corner with one wall parallel and the other perpendicular to the antenna array, the same configuration but at a 45° angle to the antenna array, and a wall parallel to the array intersecting the center of a wall perpendicular to the antenna array. Figure 30 shows the experimental setup for the test where the wall is perpendicular to the antenna array.

Figure 31 shows the images that resulted from these tests. Each image has had the specific wall configuration superimposed on the reconstructed image. It is evident from the images that the

Figure 30 - Experimental setup for early imaging tests.

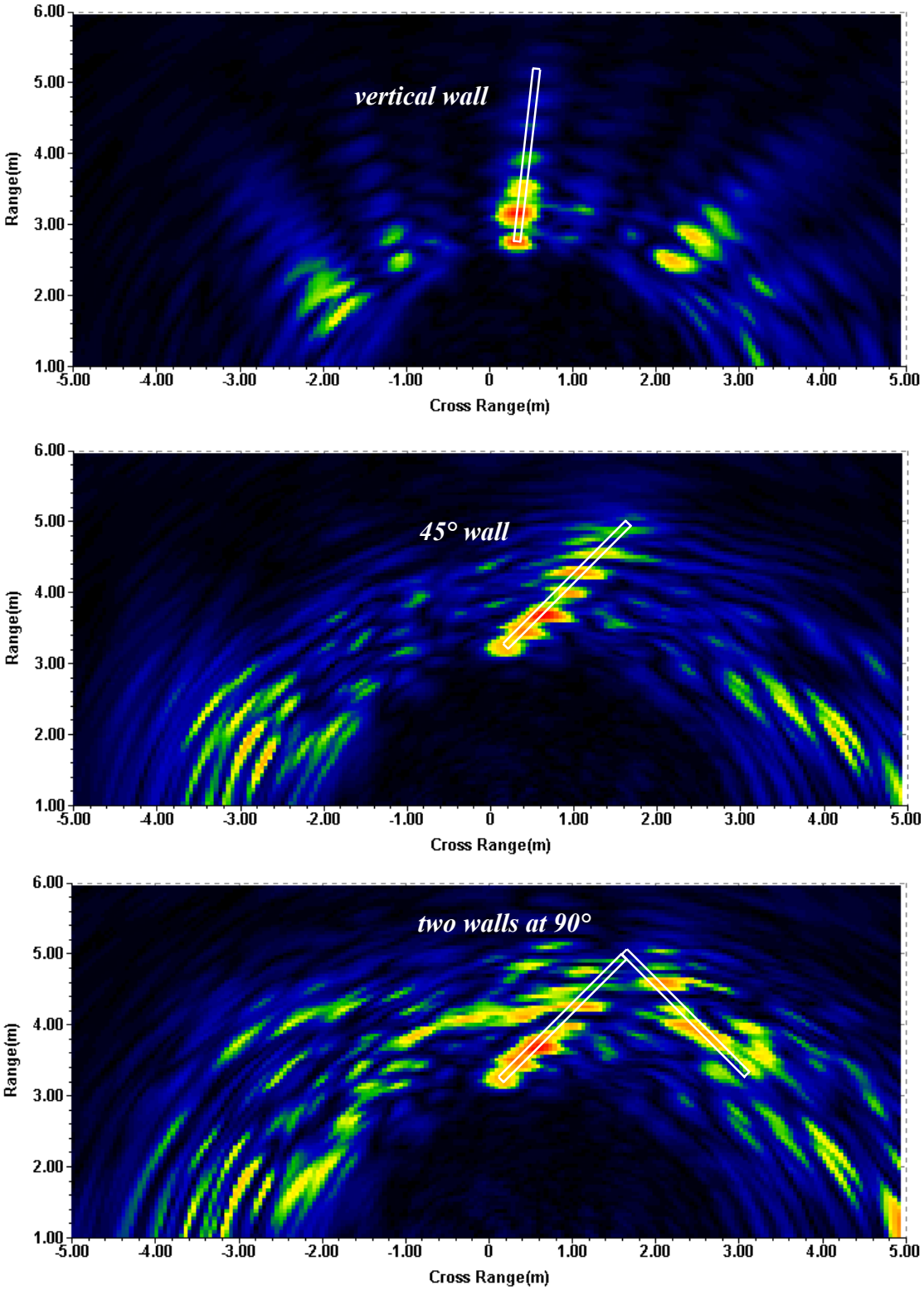

Figure 31 - Images of various interior wall configurations.

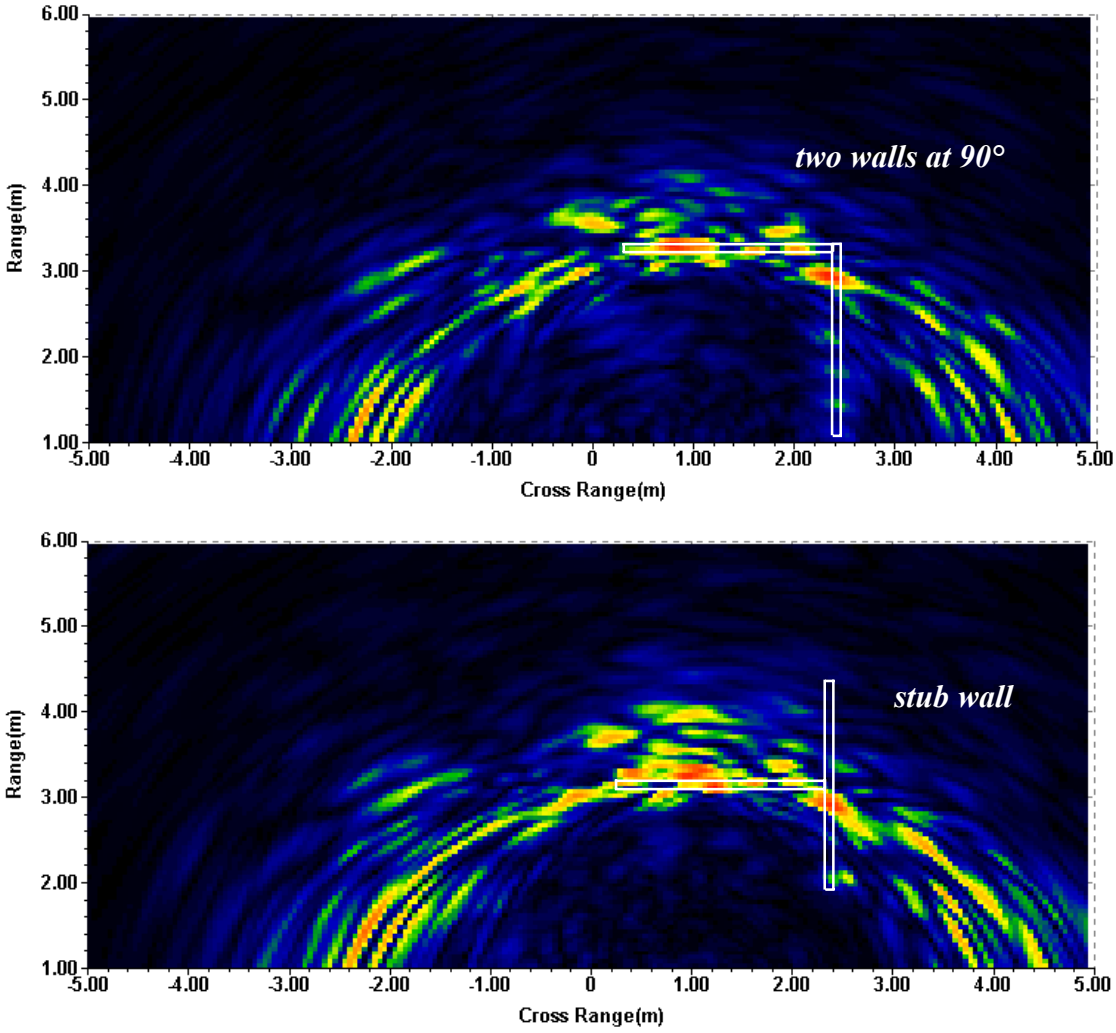

Figure 31 - Continued.

studs forming the interior structure of the wall can easily be seen. This early set of data showed two areas of emphasis for the image processing algorithms. The first was the necessity to accurately characterize the physical parameters of the sensor system. Initial attempts at forming images gave poor results. In the process of determining why, it was discovered that one of the cables in the antenna array was longer than the others and one of the channels of the antenna switchbox had partially failed resulting in a lower gain signal path. Correcting these physical parameters in the image reconstruction improved the results considerably. The other area is the appearance of ghosts in the images. This is particularly evident in the image for the wall perpendicular to the antenna array and prompted the beginning of exploration of methods for reducing this effect.

An early set of data to explore motion detection performance of the experimental system was also taken. Simulations had been performed using MATLAB of what motion detection using scene subtraction would look like. These simulations used two sets of antennas and a single point source moving away along the two element antenna array boresite. To compare performance of the radar to the simulations, we used an inflatable ball covered with aluminum foil as the point source, and set up a simple two element array in a cluttered conference room to give us a feel for how difficult multiple reflections would make the motion detection. Figure 32 shows the conference room experimental setup.

As can be seen in the figure, there were many additional sources for scattering in the conference room. In addition, on the opposite side of the left wall in the picture, there was a row of metal desks which provided a highly reflective surface. The data was taken a frame at a time, moving the foil covered ball between frames. We used MATLAB to analyze the data. Figure 33 shows a composite image from the motion detection experiment. As is evident in the composite image,

Figure 32 - Experimental setup for early motion detection tests.

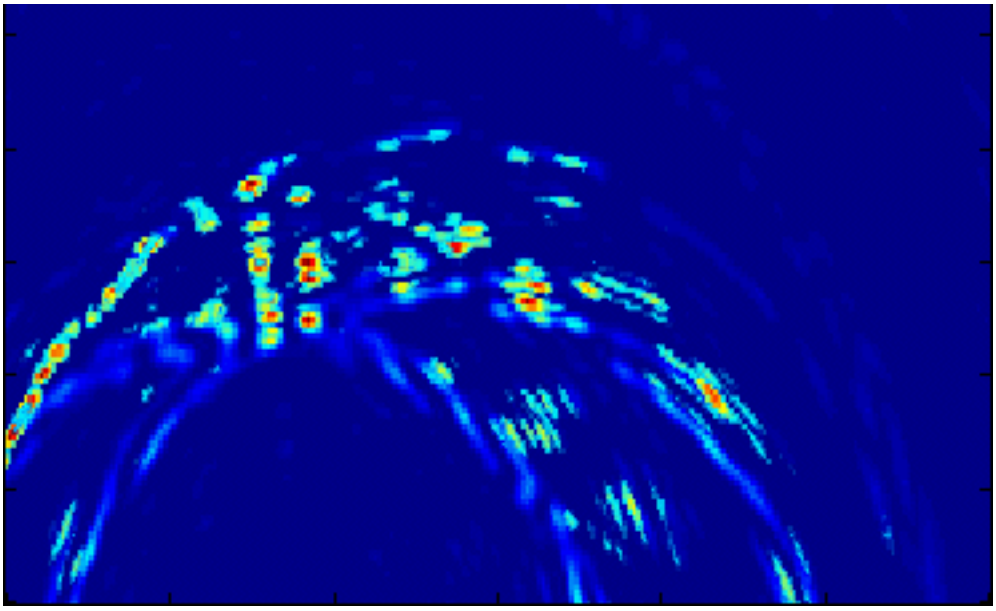

Figure 33 - Composite image of early motion detection experiments.

the reflections from other objects in the room present a challenge to the motion detection. While the trail of the ball can be seen, there are other apparent targets in the scene. Since only two antennas were used for the experiments, the false targets are more prominent than they would be for an array with a larger number of antennas. This set of experiments, though, validated the algorithmic approach and the basic algorithms were then incorporated into the radar control and interface software.

After making modifications and repairs to the experimental radar system, a set of tests was performed to determine the capability of the radar to image through concrete walls. Two different sites at UCSB were selected. The first was a large conference room shown both from the inside and outside in the photos of Figure 34.

The wall of the conference room is approximately 12” thick and made of steel reinforced, poured concrete. Since the objective of the testing was to determine how well the radar could penetrate the concrete wall, we performed background tests where there were no individuals on the other side of the wall and then several tests with individuals at different distances from the wall. Since there is a great deal of attenuation introduced by the concrete wall, the signal levels from the

people are much smaller than reflections from the wall and its internal features. During our data analysis we subtracted the background data from the data with people present in order to remove as much of the effect of the wall as possible. Figure 35 shows two images from this test series.

Figure 34 - Inside and outside of UCSB conference room test site.

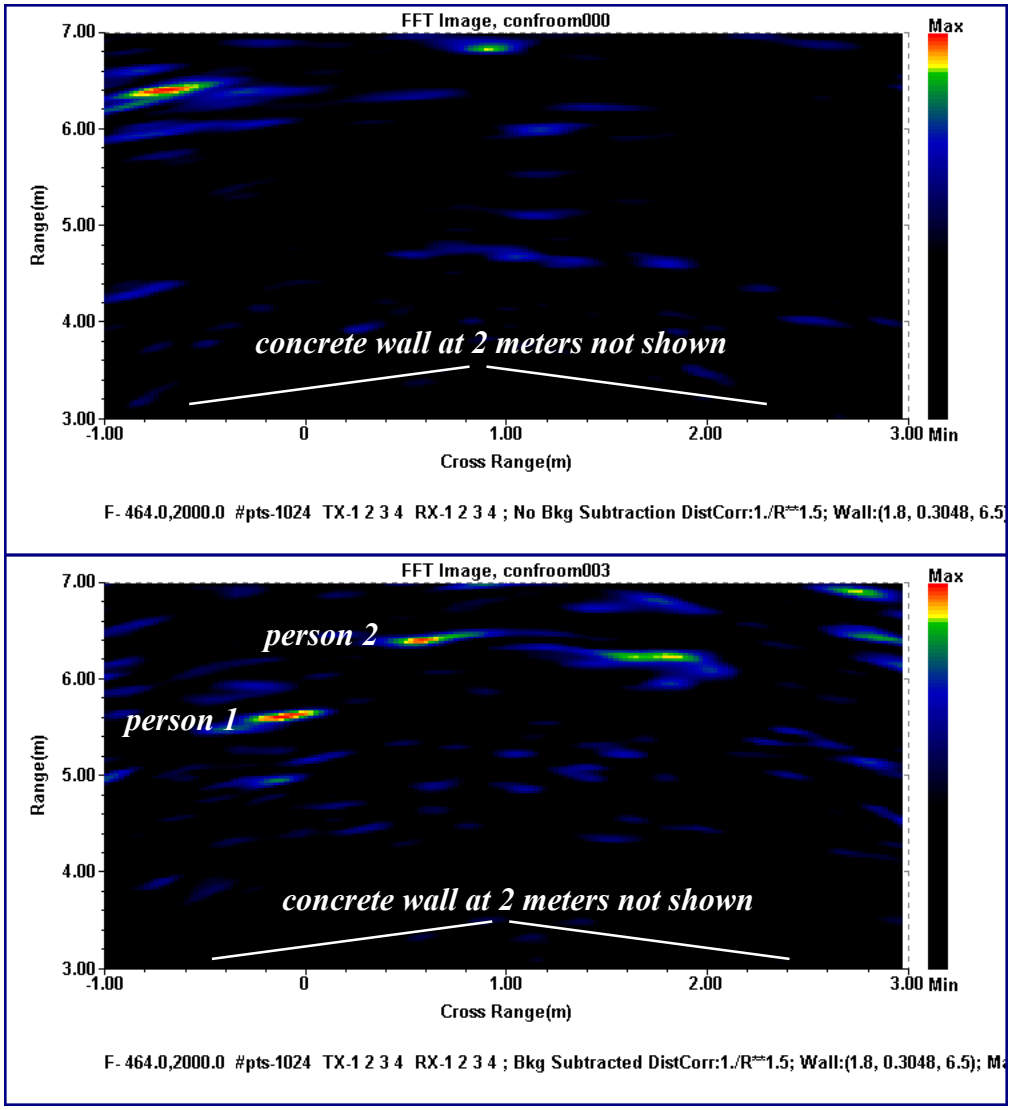

Figure 35 - Background compared with image of two individuals behind concrete wall.

The image at the top of the figure is of the area from approximately 1 meter behind the concrete wall to 5 meters behind the wall for the background scan. This image shows the positions of strong reflections from the background scan and can be used to compare with the positions of the strong reflections in the bottom image. The bottom image covers the same external area and is a data scan that contains three people in positions approximately as shown in the bottom photo of Figure 32. This scan has had the background of the top image subtracted from it. As shown in the image, there are three reflections that are in different positions than those in the background

image. Since the actual positions of the individuals were not accurately recorded, it is most likely that the two strongest reflections are from the two individuals visible in the image. The third person is not visible because he is outside the display area and his reflection is approximately at the same level as the noise.

The second test site at UCSB was a lecture hall constructed with prefabricated concrete walls approximately 8" thick. Our tests at this site had similar objectives as the conference room tests, however, we used two different imaging arrays. In addition to the experimental array with the large antennas, we used an array with smaller antennas designed for operation above 750 MHz, and modified radar electronics with an upper frequency limit of 3000 MHz. Operating at higher frequencies allows the use of a smaller and lighter imaging array, however, attenuation from the concrete also increases with frequency. These tests were designed to help us determine how much different the performance of the two frequency bands was. A photograph of the outside wall of the lecture hall and the small imaging array is shown in Figure 36.

Unfortunately, the performance of the high frequency array was poorer than expected. Since this was a diversion from our main development activity, we did not pursue this approach any further and focused all of our attention on the larger, lower frequency imaging system. Figure 37 shows

Figure 36 - Outside wall of lecture hall and high frequency imaging array.

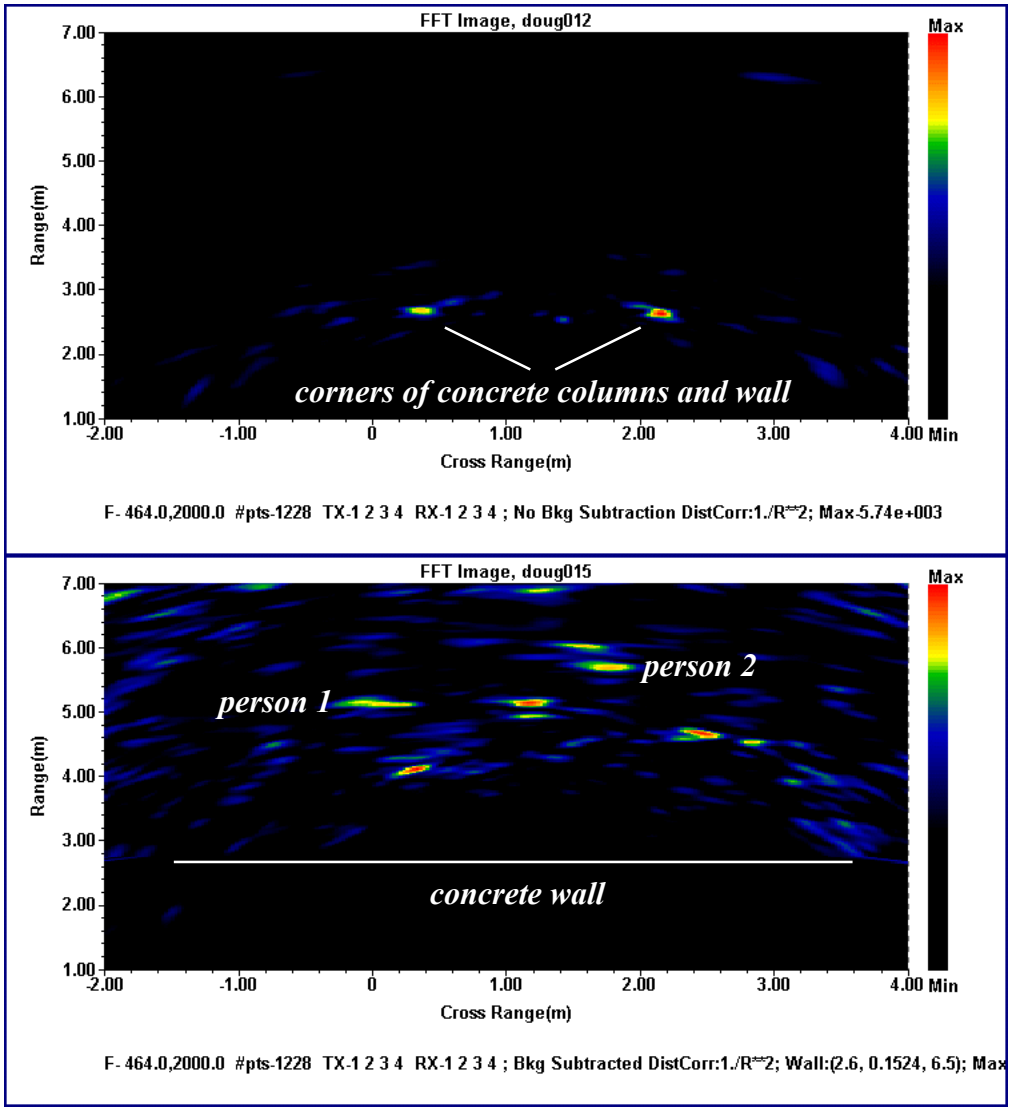

Figure 37 - Outside and inside of UCSB lecture hall wall.

two images that were taken with the larger system during this test series. The top image in the figure is of the outside of the lecture hall. The two strong reflections in the image come from the corners made by the concrete support structure and the concrete wall that can be seen in the photo of the lecture hall. The bottom image has had the background image of the wall subtracted from it and contains two people and a set of three trash cans set in a triangular pattern. While the exact positions of the individuals and the trash cans were not recorded, the reflections seen in the image are in the area where the individuals and objects were positioned.

At this point in the program experimental and simulation results were sufficient to enable us to select the design parameters for development of the brassboard imaging system. It was decided that a four antenna, linear scanned array would provide performance sufficient to demonstrate overall program goals. After the brassboard array was fabricated and assembled, performance testing began.

Initial testing with the brassboard was with the interior walls built earlier in the program positioned in an open area. Tests were performed on various configurations with one and two walls with one or two individuals standing behind them. Figure 38 shows two of the configurations that were tested. In the case of the single wall, the wall was positioned 4.6 meters in front of the imaging array and the person was behind the wall and 10 meters from the array. For the two wall case, the second wall was placed 7.2 meters in front of the array. A second person was placed approximately half way between the two walls.

Figure 39 shows the imaging results obtained from this series of tests. In (a) the person standing at 10 meters is clearly evident. In (b) a second wall has been placed in front of the person at 10 meters. Even though the return from the person is somewhat weaker, the person can still be clearly identified. In (c) a second person was placed in between the two walls. As expected, the return from this person is stronger than that from the person standing behind both walls, however, both individuals can still be seen. In all of the figures, a set of horizontal lines show the location of the walls. The lines accurately mark the edges of the walls and closely approximate the thickness of the wall.

A series of experiments to demonstrate motion detection was also performed with the two wall configuration. Because the sweep speed of the radar is too slow to capture motion at normal speeds, we reduced the number of frequencies per sweep to 256 and captured image frames approximately once every 4 seconds. In this case it was necessary to coordinate movement with the person so that there was motion only between frames. The person started out walking in front of both walls moving to the left looking from the imaging array. Upon arriving at the end of the first wall he continued around the end of the wall, reversed direction and proceeded to move between both walls to the other end of the walls. At the other end, he again reversed direction, and walked behind the second wall until reaching the left end again. As seen in the figure, the imaging array was able to very robustly detect motion the entire time and through a total of two walls.

Figure 38 - Interior wall test configuration .

Based on these initial results, it was decided to move the brassboard array to a different environment where other types of image and motion detection tests could be performed. We returned to UCSB and set up the array outside a double wide trailer that is currently being used as an administrative area. Figure 41 shows the test setup for the imaging and motion detection experiments. The array was set up outside the trailer approximately 4.5 meters from the wall. While the exterior wall shows up quite well, the interior structure is less well defined. Figure 43 shows the

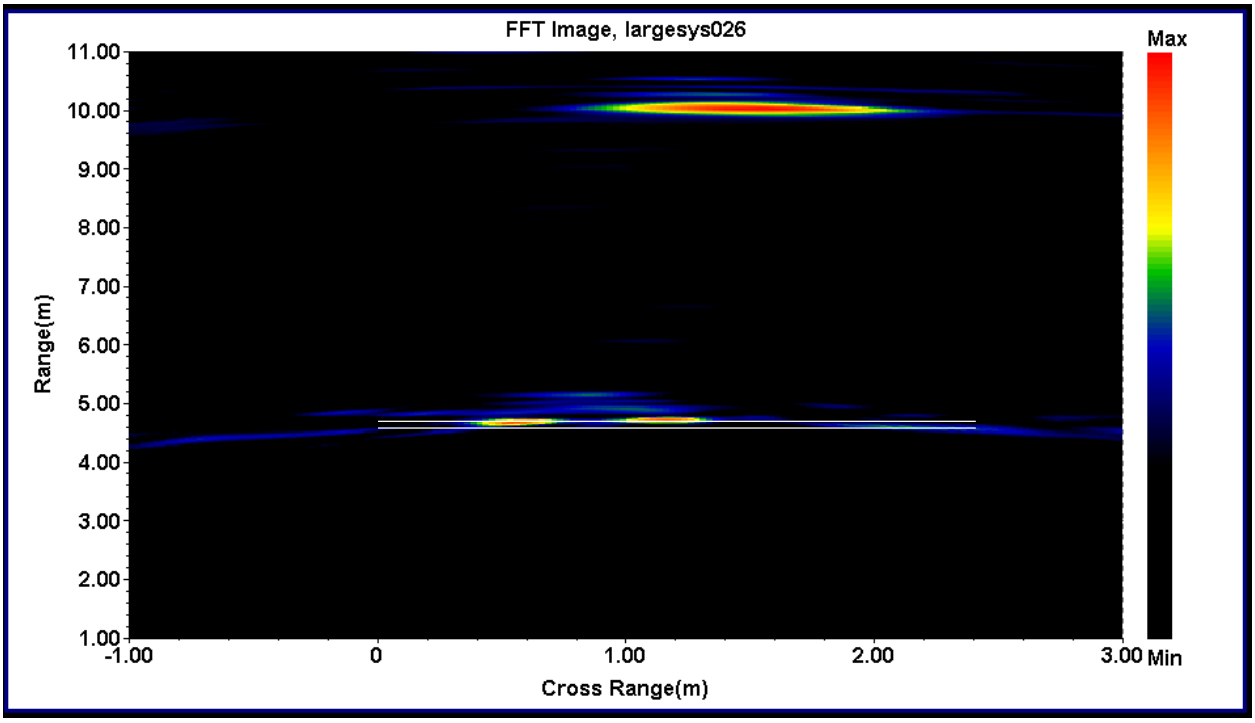

(a)

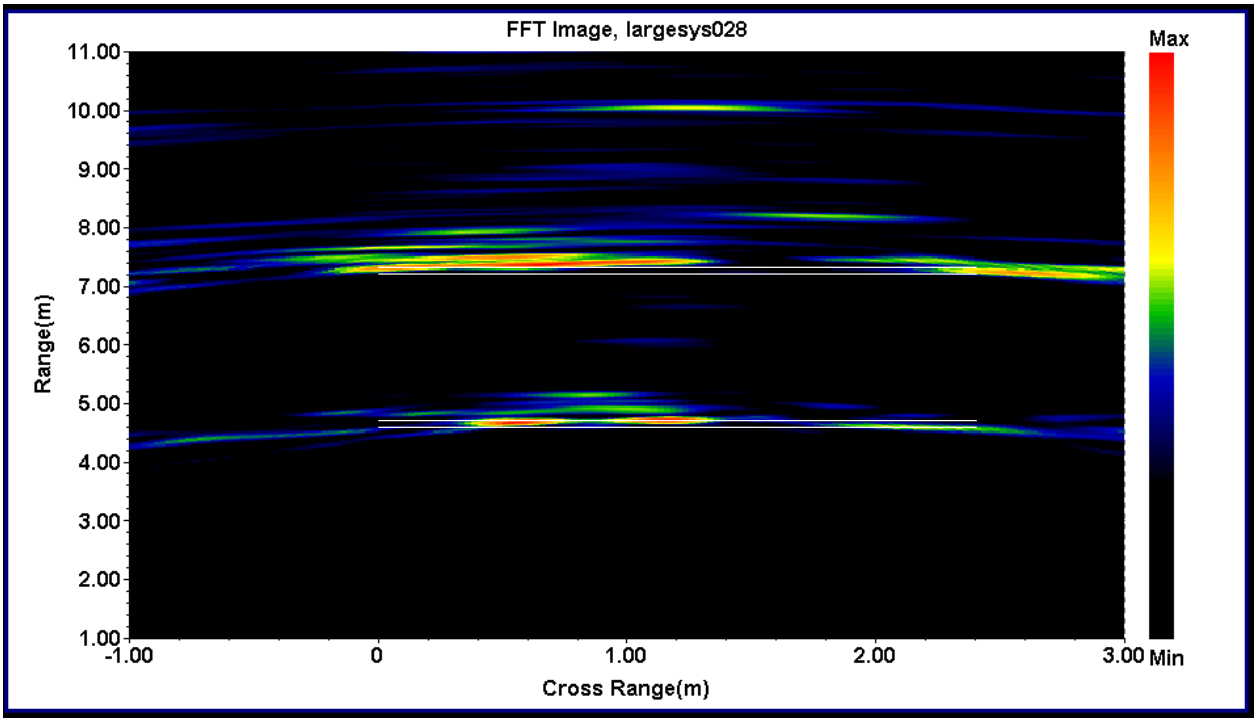

(b)

Figure 39 - (a) Person behind one interior wall, (b) Person behind two interior walls, (c) One person behind a single wall, and one person behind two walls.

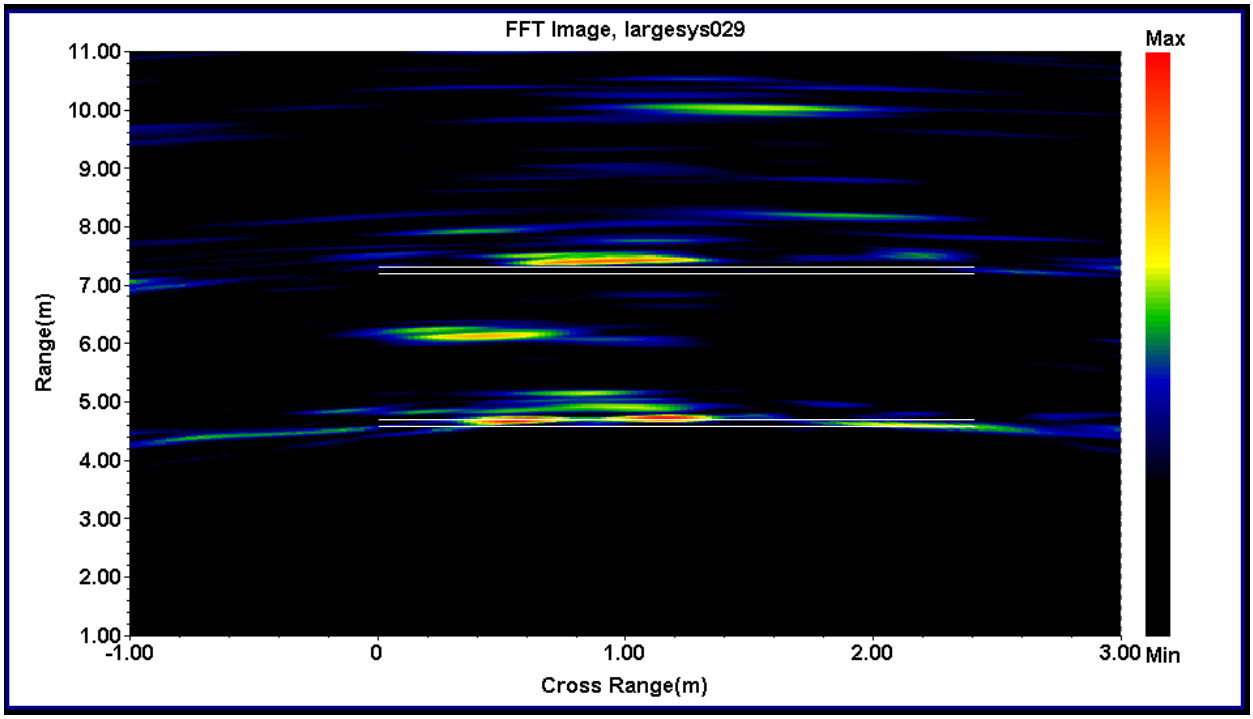

(c)

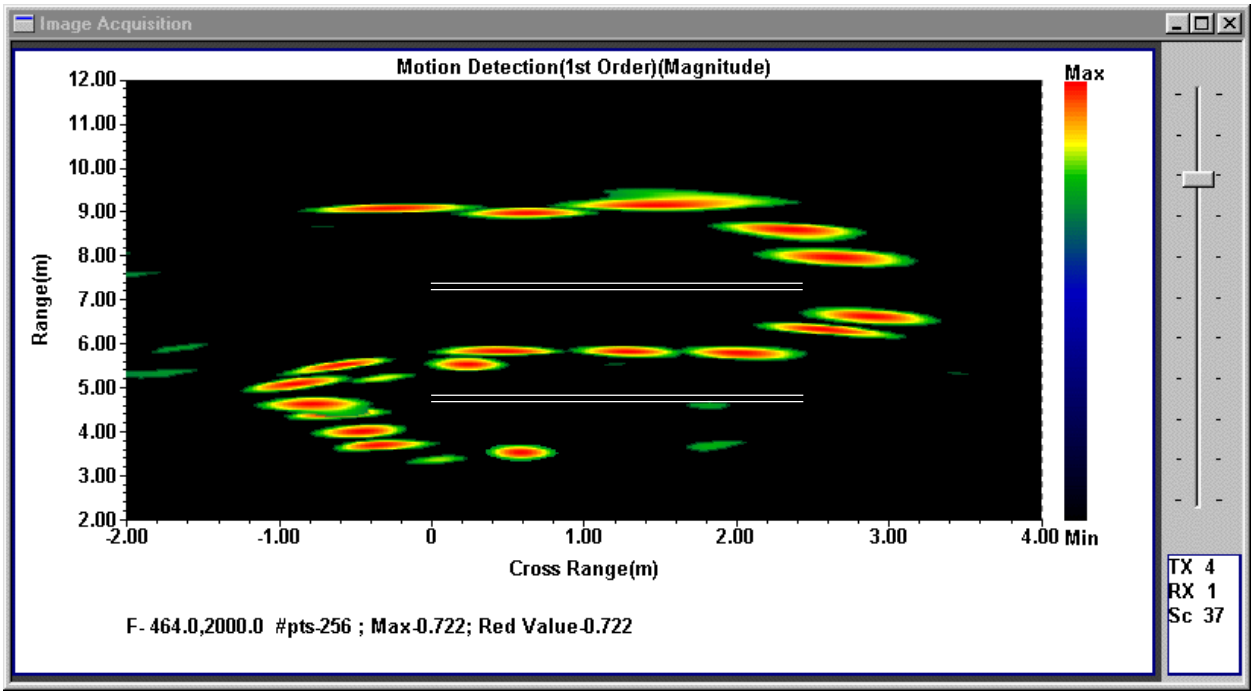

Figure 40 - Composite image of motion of a person walking behind interior walls.

Figure 41 - Double wide trailer at UCSB used for imaging and motion detection testing.

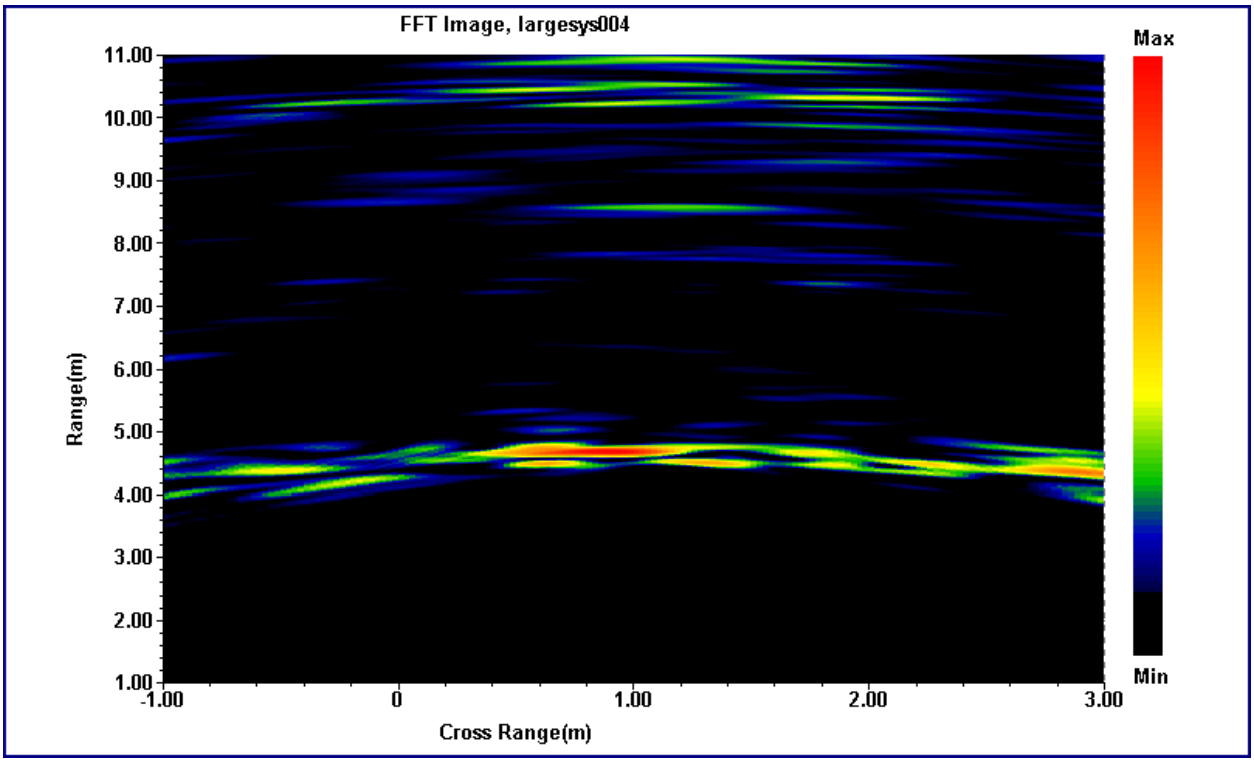

Figure 42 - Image of trailer outside wall and interior.

interior structure just behind the outside wall. The small office shown in the photo is directly in front of the array. It is filled with metal bookshelves and a desk arranged around the inside of the office space. Our motion detection testing took place in this interior office. Since there was little room to move around, the individual moved back and forth between the outside and interior wall of the office. Figure 44 shows a composite image of the motion detected in the office through the exterior wall of the person walking away from the array and toward the back of the trailer office wall. Figure 45 shows a composite image of the motion of the person on the way back toward the front of the trailer. Two images are shown for clarity since both paths were the same.

Figure 43 - Trailer interior configuration.

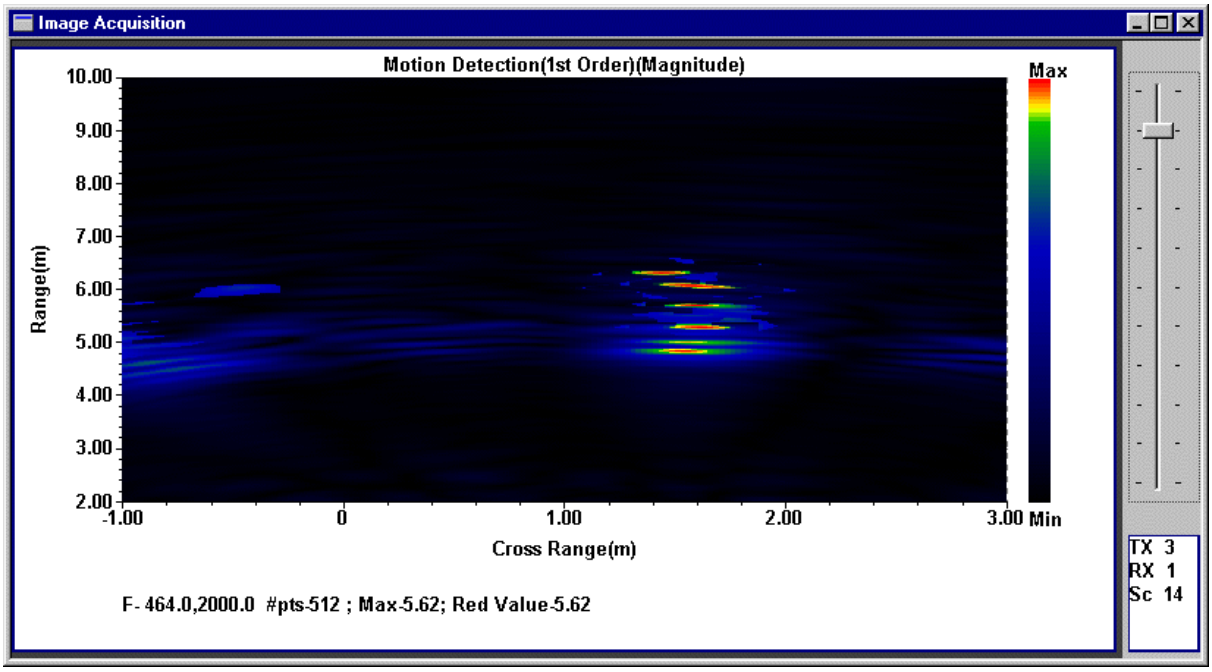

Figure 44 - Composite image showing person walking toward back of trailer office.

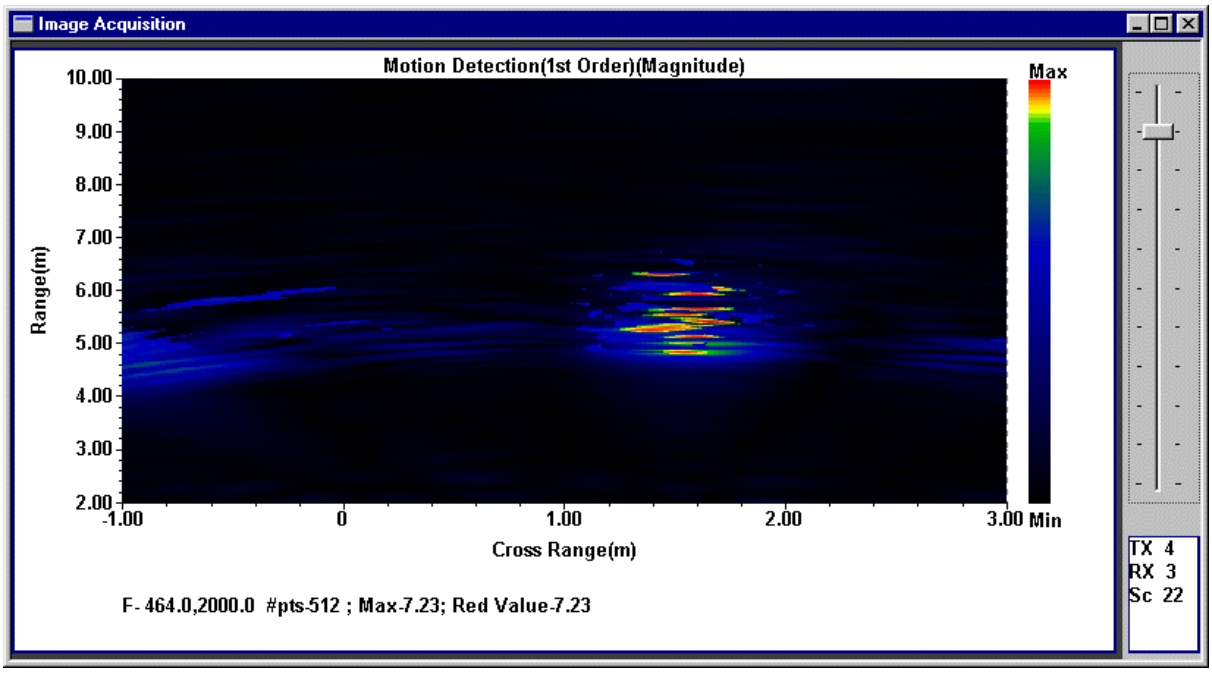

Figure 44 - Composite image showing person walking toward front of trailer office.

A set of tests to determine whether it was possible to detect motion behind twelve inches of steel reinforced, poured concrete was also performed. Only 256 frequency points were taken for each sweep in order to minimize the data collection time. Unfortunately, the signal to noise ratio when using this number of points is lower than for a sweep with more points. While it appeared that motion could be detected, the performance was poor due to the low signal levels and high attenuation of the concrete.

The last set of performance tests with the brassboard was a demonstration of the improvement in cross range resolution that can be obtained by using a longer antenna array. For this set of tests, we returned to the open area and used the interior walls in various configurations. Two arrays were set up end to end and used as a single, linearly scanned, eight element array. Figure 45 is an image of two interior walls that are parallel to the imaging array and are approximately 4.5 and 7.5 meters in front of the array. In contrast with Figure 39(b), the individual studs in the first wall are clearly seen, as are features of the second wall.

Figure 46 shows the same configuration with a third perpendicular wall added at the right end of the two parallel walls making a three sided room. The shape of the room is clear in the image. These images show the improvement in cross range resolution that can be obtained by using a

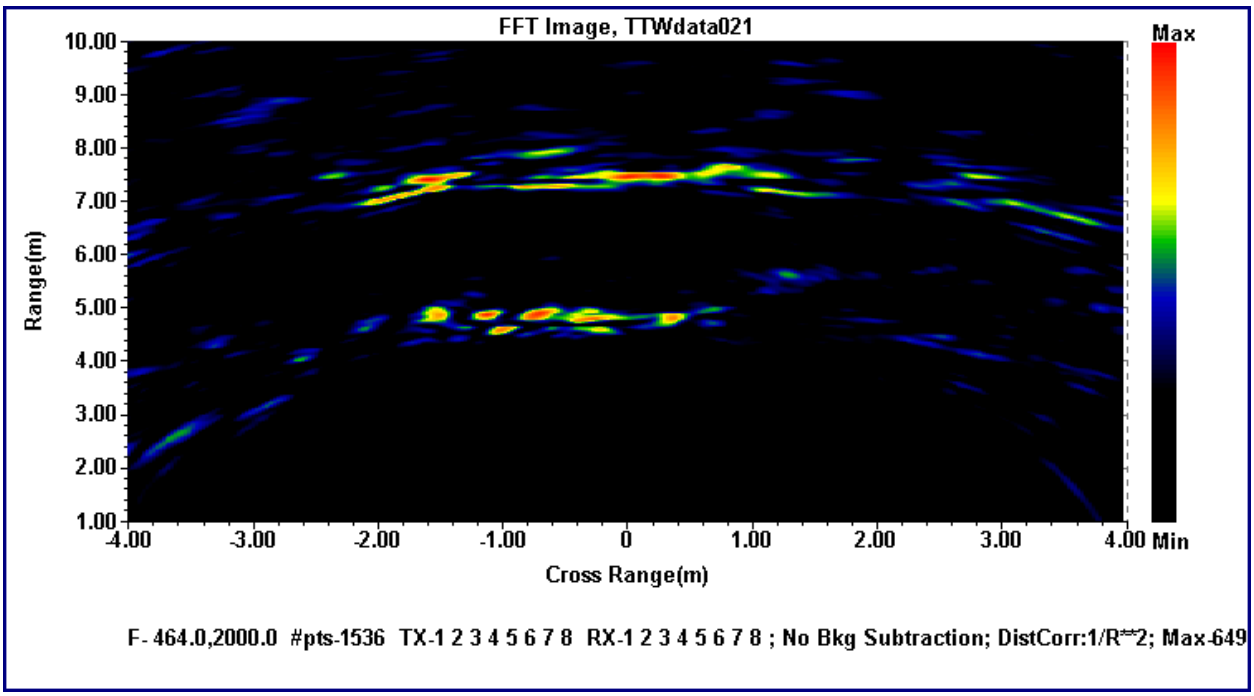

Figure 45 - Image of two parallel walls using extended length imaging array.

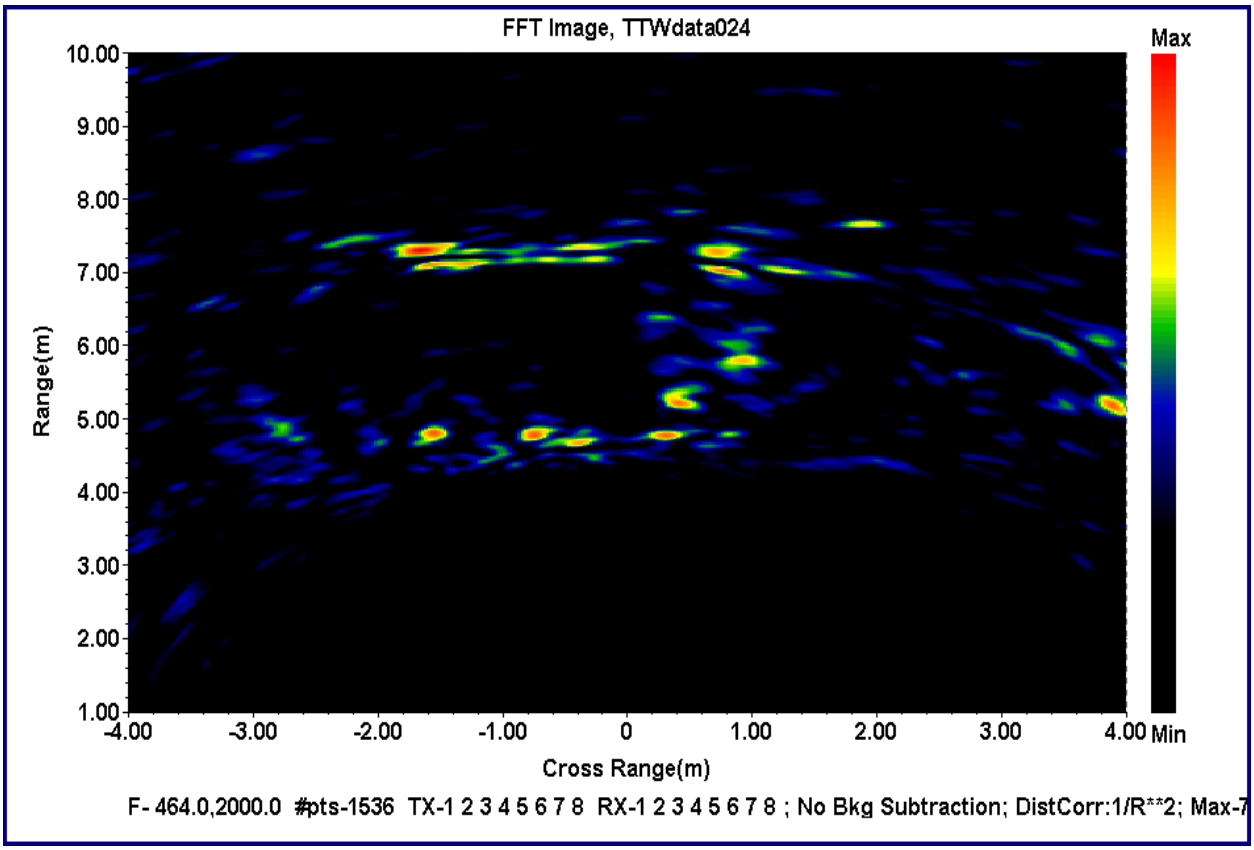

Figure 46 - Image of one perpendicular and two parallel walls .

longer array. As indicated earlier, this same resolution could also be achieved by keeping an array of the same length but increasing the lowest frequency of operation of the radar.

Figure 47 shows a configuration where the third wall is removed from the end of the two parallel walls, and placed behind them to form a series of three parallel walls. The third wall is far enough away from the array that the studs are not able to be resolved but now blur and merge showing a relatively continuous line. Finally, Figure 49 shows the same image but in an image map that extends out to 30 meters. This is the program goal distance. In the figure, the three parallel walls are readily seen in the foreground. The strong reflection at approximately 22.5 meters is a concrete block that is buried in a hill behind the three walls. It is seen through all three walls.

We performed motion detection tests with this configuration, too. To do so, however, we only collected 256 frequency points per sweep. Unfortunately, subsequent analysis of the data showed that we had exceeded the unambiguous range limit during the testing. This resulted in aliasing of the data and failure of the motion detection algorithms. By the time the data analysis was complete and this problem discovered, there was no longer any time or money to repeat the tests.

Conclusion

The goals of this program were to develop a brassboard imaging radar 1) suitable for portable, fixed in place operation with a 100 foot range, 2) capable of reconstructing an image of the interior of a building, and 3) capable of detecting motion of people within the building. These goals have been met.

The brassboard antenna array and radar electronics have been integrated into a collapsing structure that weighs less than 20 pounds and is small enough that it can be carried by a single individual when in the fully collapsed configuration. A laptop computer can be used to perform all radar control and display functions. Cooperative efforts with another program have demonstrated that the range of the radar in an open environment is approximately 225 feet. The range achieved in the case where multiple walls must be penetrated will be a function of the number and type of walls. We have demonstrated detection of an individual on this other program at a range of 40 meters (130 feet) through approximately 80 feet of dense woody brush.

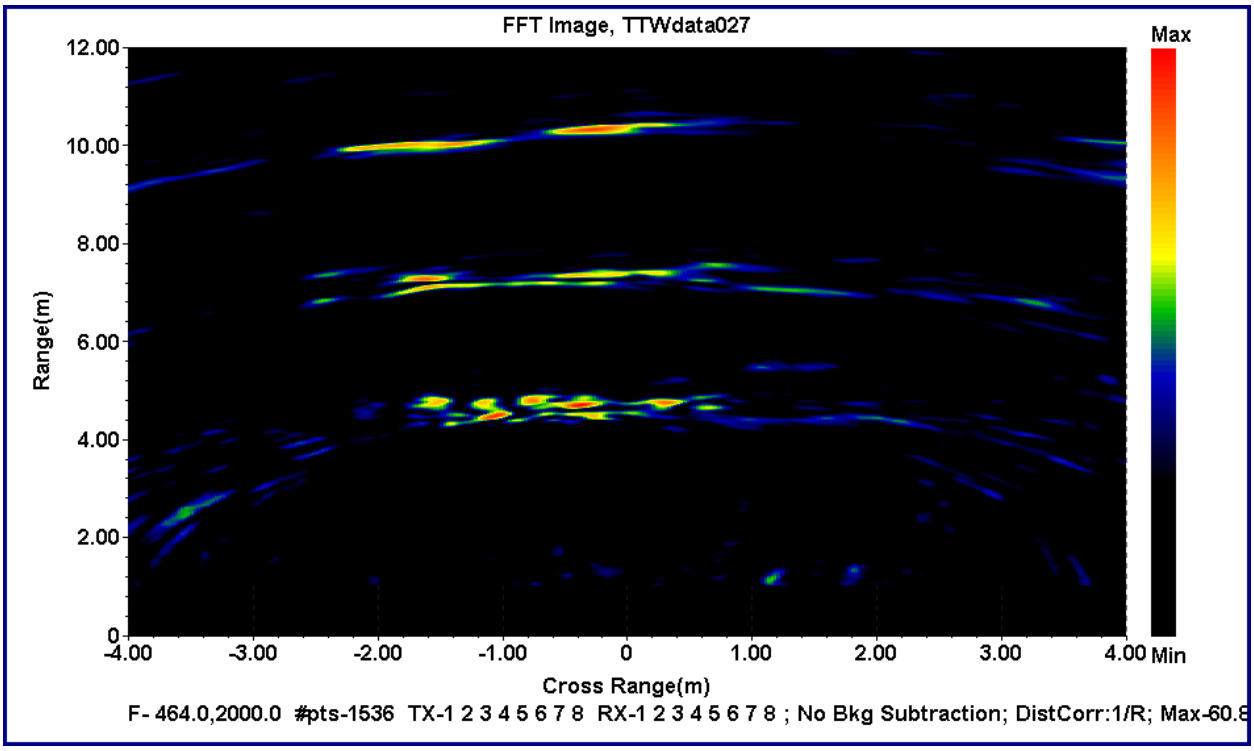

Figure 48 - Image of three parallel walls using extended length imaging array.

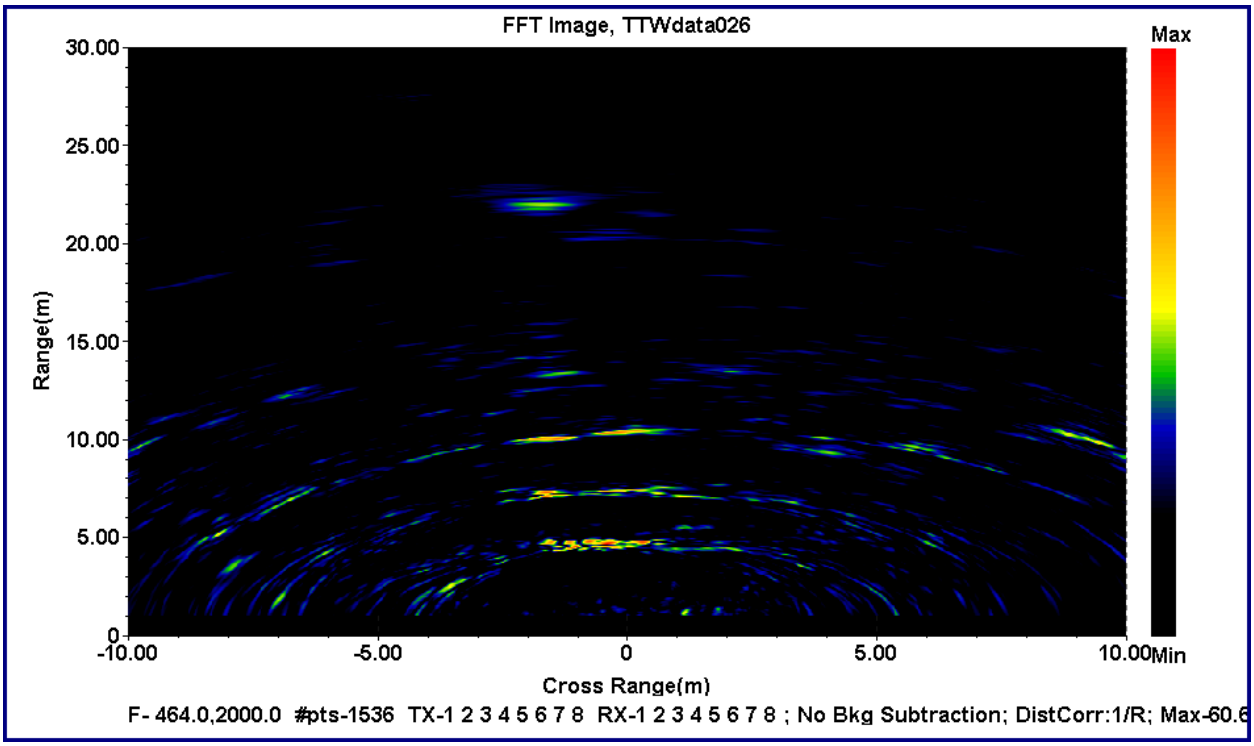

Figure 49 - Expanded area image showing three parallel walls.

Our experiments with walls typical of most buildings have shown that the radar is capable of seeing through walls and forming images of the structure. Resolution of these images is a function of the distance from the radar, the frequency of operation, and the length of the radar imaging array. Because the frequencies needed to be able to penetrate building materials are low, the images formed by the radar are not optical quality. They are, however, good enough to improve tactical awareness in operational environments.

We have demonstrated that the brassboard can be used to detect the motion of individuals through multiple interior walls using coherent scene subtraction. Concrete walls present a more difficult challenge, although our experiments suggested that a system with a higher signal to noise ratio would be able to detect motion under these conditions as well.

Both image quality and motion detection results were affected by the use of a preexisting radar for the brassboard. Improving its speed of operation and reducing its internal noise will lead to large improvements in both imaging and motion detection performance. We performed some preliminary design and breadboard experiments on methods of improving performance and have concluded that it is possible to achieve image formation at video frame rates through redesign of the hardware. Our design activities have identified existing, cost effective, commercial technology sufficient to implement these improvements.

Our program activities have addressed the major technical uncertainties associated with imaging through walls with a static antenna array. It is possible to make a long array that is light and portable. Tomographic imaging algorithms can be applied to make images of the interior of building structures that are operationally acceptable. And the electronics technology exists to build an imaging radar that can form images at video frame rates enabling it to image and detect motion on an operationally relevant time scale. These activities have identified a low risk path to development of an operationally relevant, through- the-wall imaging system.